
Atomic Diffusion Models for Small Molecule Structure Elucidation from NMR Spectra

Ziyu Xiong
Princeton University
ziyux@princeton.edu

Yichi Zhang
Princeton University
zycddd@princeton.edu

Foyez Alauddin
Princeton University
fa1073@alumni.princeton.edu

Chu Xin Cheng
California Institute of Technology
ccheng2@alumni.caltech.edu

Joon Soo An
Princeton University
ahnjunsoo@princeton.edu

Mohammad R. Seyedsayamdost
Princeton University
mrseyed@princeton.edu

Ellen D. Zhong
Princeton University
zhonge@princeton.edu

Abstract

Nuclear Magnetic Resonance (NMR) spectroscopy is a cornerstone technique for determining the structures of small molecules and is especially critical in the discovery of novel natural products and clinical therapeutics. Yet, interpreting NMR spectra remains a time-consuming, manual process requiring extensive domain expertise. We introduce CHEFNMR (CHEMical Elucidation From NMR), an end-to-end framework that directly predicts an unknown molecule’s structure solely from its 1D NMR spectra and chemical formula. We frame structure elucidation as conditional generation from an atomic diffusion model built on a non-equivariant transformer architecture. To model the complex chemical groups found in natural products, we generated a dataset of simulated 1D NMR spectra for over 111,000 natural products. CHEFNMR predicts the structures of challenging natural product compounds with an unsurpassed accuracy of over 65%. This work takes a significant step toward solving the grand challenge of automating small-molecule structure elucidation and highlights the potential of deep learning in accelerating molecular discovery. Code is available at this [https URL](https://github.com/zyxiong/CHEFNMR).

1 Introduction

The molecules that sustain life come in several forms: large biopolymers such as DNA, RNA, and proteins described by our genetic code, and small molecules, which form complex metabolic pathways and influence all aspects of biology. A category of small molecules, known as secondary metabolites or **natural products**, describes those that are secreted into the environment where they serve myriad functions, such as signaling and chemical warfare. Because of these roles, natural products have delivered more than half of the FDA-approved small-molecule agents, including the majority of antibiotics and antitumor drugs in current clinical use, such as penicillin, taxol, and other blockbuster drugs such as lovastatin and semaglutide [48, 14, 68, 58].

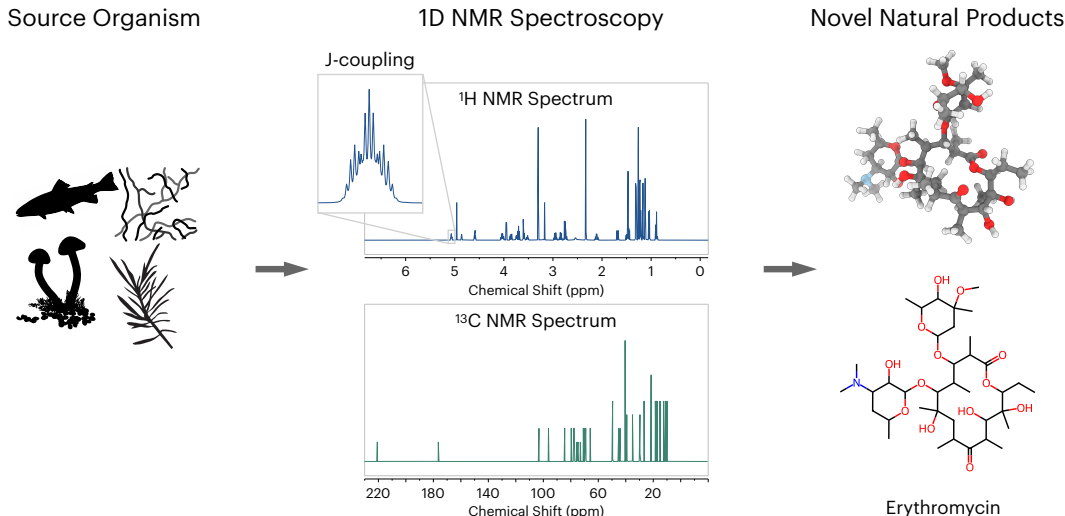


Figure 1: **Natural products** are small molecules secreted by natural sources such as plants, animals, and microorganisms (left). To identify an unknown molecule’s structure, 1D NMR spectroscopy measures peaks corresponding to each proton (^1H) or carbon (^{13}C) atom (middle). The resulting *chemical shifts* (x-axis locations), *peak intensities*, and *J-coupling* (splitting patterns) encode information on chemical groups and connectivities, from which the molecular structure can be deduced (right).

The functions of small molecules are intrinsically linked to their molecular structures, which govern their chemical and biological reactivity. Very recently, deep learning methods have revolutionized the prediction of a protein’s 3D structure from its amino acid sequence encoded in the genome [30, 2]. Small molecules, by contrast, are neither directly genetically encoded nor repeating polymers. Structure elucidation therefore relies on *de novo* experimental methods for every new molecule, making the discovery of cellular metabolites, essential molecules, antibiotics, and other therapeutics a slow and tedious process [8, 48, 18].

Nuclear Magnetic Resonance (NMR) spectroscopy is a cornerstone technique for small molecule structure elucidation. This experimental method provides information regarding the connectivity and local environment of, typically, each proton (^1H) and carbon (^{13}C) in a molecule, thus allowing the structure of a molecule to be deduced. However, the inverse problem of inferring the chemical structure from these spectral measurements is a challenging puzzle, which largely proceeds manually and requires significant time and expertise, even with computational assistance [8]. Consequently, automating molecular structure elucidation directly from raw 1D NMR spectra would significantly accelerate progress in chemistry, biomedicine, and natural product drug discovery [56, 47, 77, 42, 17].

With the rise of deep learning approaches applied to molecules, diffusion generative models [20, 59, 32] have emerged as powerful tools for tasks such as small molecule generation [21, 46, 69, 40], ligand-protein docking [10, 57], and protein structure prediction [2, 73] and design [25, 70, 15]. While early approaches emphasize 3D geometric symmetries via equivariant networks, recent trends suggest that non-equivariant transformers scale more effectively with model and data size and better capture 3D structures with data augmentation [69, 2].

In this work, we tackle the challenging task of NMR structure elucidation for complex natural products. We introduce CHEFNMR (CHEmical Elucidation From NMR), an end-to-end diffusion model designed to infer an unknown molecule’s structure from its 1D NMR spectra and chemical formula. CHEFNMR processes NMR spectra using a hybrid transformer with a convolutional tokenizer designed to capture multiscale spectral features, which are then used to condition a Diffusion Transformer [49] for 3D atomic structure generation. To scale to the complex chemical groups found in natural products, we curate SpectraNP, a large-scale dataset of synthetic 1D NMR spectra for 111,181 complex natural products (up to 274 atoms), significantly expanding the chemical complexity of prior datasets (≤ 101 atoms) [22, 4]. We compare CHEFNMR against chemical language model-based and graph-based formulations and demonstrate state-of-the-art accuracy across multiple synthetic and experimental benchmarks.

2 Background

NMR spectroscopy is a widely used analytical technique in chemistry for determining the structures of small molecules and biomolecules. A typical one-dimensional (1D) NMR experiment measures the response of all spin-active nuclei of a given type, for example hydrogen (^1H) or isotopic carbon (^{13}C), to radiofrequency pulses in a strong magnetic field. The resulting spectrum consists of peaks from chemically distinct nuclei, where peak positions (i.e., chemical shifts), intensities, and fine splitting patterns (i.e., J -coupling) reflect local chemical environments and connectivities of the nuclei.

Formally, let the observed spectrum be a real-valued signal $S(\delta) : \mathbb{R} \rightarrow \mathbb{R}$, where δ denotes the chemical shift (in parts per million, ppm) along the x-axis. The signal can be modeled as a sum over N resonance peaks corresponding to each spin-active nucleus:

$$S(\delta) = \sum_{i=1}^N A_i \cdot L(\delta; \delta_i, \gamma_i) + \epsilon(\delta) \quad (1)$$

where A_i is the intensity (amplitude) of the i -th peak, δ_i is the chemical shift (peak center), and γ_i is the linewidth (related to relaxation) of the peak. $L(\delta; \delta_i, \gamma_i)$ is the normalized Lorentzian line shape:

$$L(\delta; \delta_i, \gamma_i) = \frac{1}{\pi} \cdot \frac{\gamma_i}{(\delta - \delta_i)^2 + \gamma_i^2} \quad (2)$$

and $\epsilon(\delta)$ models additive noise (e.g., Gaussian white noise or baseline drift). J -coupling refers to the splitting of the signal for a given nucleus into a sum of multiple peaks when nearby atoms interact:

$$S(\delta) = \sum_{i=1}^N \sum_{k=1}^{M_i} A_{ik} \cdot L(\delta; \delta_{ik}, \gamma_{ik}) + \epsilon(\delta) \quad (3)$$

where M_i is the number of split components for the i -th nucleus, and δ_{ik} encodes the shifted peak positions. J -coupling occurs when other spin-active nuclei are within 2–4 edges in the molecular graph, and the signal splits into $M_i = m + 1$ components assuming m interacting nuclei. See Figure 1 for an example.

Together, these features encode rich information about the types of chemical groups present and their connectivities, enabling chemists to deduce the underlying molecular structure. For example, certain chemical groups produce peaks that appear at an established range (e.g., aromatic ring-protons are detected at 6.5–8 ppm), whose exact location depends on the amount of chemical shielding from nearby atoms in a given molecule. These patterns, in addition to experimental noise due to the instrument, impurities, and solvent effects, make the inverse problem of deducing structure an extremely challenging task. NMR structure elucidation thus typically relies on additional information from 2D NMR experiments, prior information on the substructures present, or chemical formula from high-resolution mass spectrometry [7] combined with isotopic abundance and distribution patterns. In this work, we use the chemical formula as an auxiliary input, as it is typically the most readily obtainable among common priors and effectively constrains the space of candidate molecular structures for complex natural products.

3 Method

In this section, we present CHEFNMR, an end-to-end diffusion model for molecular structure elucidation from 1D NMR spectra and chemical formula. Our approach consists of two key components: NMR-ConvFormer for spectral embedding (Section 3.1) and a conditional diffusion model for 3D atomic coordinate generation (Section 3.2).

In CHEFNMR, we represent molecule-spectrum pairs as $(\mathbf{A}, \mathbf{X}, \mathcal{S})$, where $\mathbf{A} \in \{0, 1\}^{N \times d_{\text{atom}}}$ denotes the one-hot encoding of atom types for a molecule with N atoms and d_{atom} possible atom types, $\mathbf{X} \in \mathbb{R}^{N \times 3}$ represents the 3D atomic coordinates, and $\mathcal{S} = (\mathbf{s}_\text{H}, \mathbf{s}_\text{C})$ contains the NMR spectra, specifically the ^1H spectrum $\mathbf{s}_\text{H} \in \mathbb{R}^{d_\text{H}}$ and the ^{13}C spectrum $\mathbf{s}_\text{C} \in \mathbb{R}^{d_\text{C}}$. Our objective is to generate the 3D coordinates \mathbf{X} conditioned on the atom types \mathbf{A} (i.e., chemical formula) and the spectra \mathcal{S} by sampling from the conditional probability distribution $p(\mathbf{X}|\mathbf{A}, \mathcal{S})$.

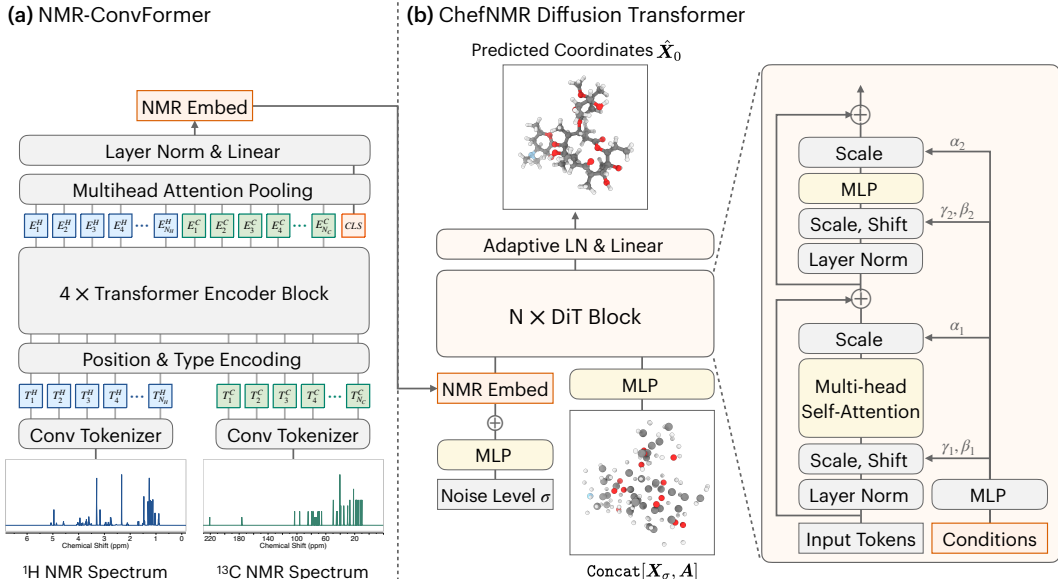


Figure 2: Overview of the CHEFNMR architecture. **(a)** NMR-ConvFormer processes 1D NMR spectra into a vector embedding using the convolutional tokenizer, transformer encoder, and multihead attention pooling (MAP). **(b)** Diffusion Transformer predicts clean 3D coordinates \hat{X}_0 from atom tokens formed by concatenating noisy coordinates X_σ and atom types A , conditioned on the spectral embedding and noise level σ via adaptive layer normalization [49].

3.1 NMR-ConvFormer: A Hybrid Convolutional Transformer for NMR spectral embedding

To effectively condition the generative process on the NMR spectra \mathcal{S} , we propose NMR-ConvFormer, an encoder designed to capture both local spectral features and global correlations within and between the ^1H and ^{13}C spectra, as shown in Figure 2(a). Unlike prior methods that rely solely on 1D convolutions [22, 45] or transformers with simple patching [67, 63], NMR-ConvFormer uses a hybrid approach, combining a convolutional tokenizer for local feature extraction and a transformer encoder for modeling complex intra- and inter-spectral dependencies.

Convolutional Tokenizer. Each input spectrum (^1H and ^{13}C) is processed independently by a convolutional tokenizer comprising two 1D convolutional layers with ReLU and max-pooling, similar to [22]. This reduces sequence length while increasing channel dimensions, summarizing local patterns like peak intensity and splitting. The output is linearly projected to dimension D_{encoder} , yielding token sequences of shape (T, D_{encoder}) .

Transformer Encoder. The token sequence, augmented with positional and type embeddings, is processed by a standard transformer encoder comprising multi-head self-attention and feed-forward networks with pre-layer norm and residuals. Self-attention captures patterns within each NMR spectrum and across different spectra, such as related peaks in a ^1H spectrum or matching signals from the same chemical group in both ^1H and ^{13}C spectra.

Multihead Attention Pooling (MAP). We use MAP [37, 79] to obtain a fixed-size spectral embedding. A learnable [CLS] token prepended to the encoder output sequence aggregates information via a final self-attention layer. The resulting [CLS] token state, after layer normalization and linear projection, serves as the conditioning vector $z_S \in \mathbb{R}^{D_{\text{hidden}}}$ for the diffusion model. Dropout is applied at multiple stages to mitigate overfitting. See Appendix D.2 for detailed hyperparameter settings.

3.2 Conditional 3D Atomic Diffusion Model

Training Objective. We adapt the EDM diffusion framework to conditional 3D molecular generation [32]. The model D_θ is trained to predict clean 3D coordinates X_0 from noisy inputs $X_\sigma = X_0 + n$, where $n \sim \mathcal{N}(0, \sigma^2 I)$ and the noise level σ is sampled from a pre-defined

distribution $p(\sigma)$. Given \mathbf{X}_σ , σ , atom types \mathbf{A} , and spectral embedding \mathbf{z}_S , the model minimizes:

$$\mathcal{L}_{\text{diffusion}} = \mathbb{E}_{\substack{(\mathbf{X}_0, \mathbf{A}, \mathbf{z}_S) \sim p_{\text{data}}, \\ \sigma \sim p(\sigma), \mathbf{n} \sim \mathcal{N}(\mathbf{0}, \sigma^2 \mathbf{I})}} \left[\lambda(\sigma) \mathcal{L}_{\text{MSE}}(\hat{\mathbf{X}}_0, \mathbf{X}_0) + \mathcal{L}_{\text{smooth_lddt}}(\hat{\mathbf{X}}_0, \mathbf{X}_0) \right], \quad (4)$$

where $\hat{\mathbf{X}}_0 = D_\theta(\mathbf{X}_\sigma; \sigma, \mathbf{A}, \mathbf{z}_S)$ are the predicted coordinates.

The MSE loss, $\mathcal{L}_{\text{MSE}} = \|\hat{\mathbf{X}}_0 - \mathbf{X}_0\|_2^2$, enforces global structure alignment. To ensure local geometric accuracy (e.g., bond lengths), crucial for chemical validity and often poorly captured by MSE alone, we add a smooth Local Distance Difference Test (LDDT) loss [43], adapted from AlphaFold3 [2]. The LDDT score is computed over all distinct atom pairs (i, j) :

$$\text{LDDT}(\hat{\mathbf{X}}_0, \mathbf{X}_0) = \frac{1}{N(N-1)} \sum_{i \neq j} \epsilon_{ij}, \quad \text{where} \quad \epsilon_{ij} = \frac{1}{4} \sum_{k=1}^4 \text{sigmoid}(t_k - |\hat{d}_{ij} - d_{ij}|). \quad (5)$$

Here, $\hat{d}_{ij} = \|\hat{\mathbf{x}}_i - \hat{\mathbf{x}}_j\|_2$ and $d_{ij} = \|\mathbf{x}_{0,i} - \mathbf{x}_{0,j}\|_2$ are the predicted and true distances, respectively. Thresholds $t_k \in \{0.5, 1.0, 2.0, 4.0 \text{ \AA}\}$ specify allowable deviations between predicted and true distances when evaluating prediction accuracy. The smooth LDDT loss is $\mathcal{L}_{\text{smooth_lddt}} = 1 - \text{LDDT}$, encourages local geometric fidelity by penalizing pairwise deviations. The combined loss promotes both global alignment and local chemical validity.

Random Coordinate Augmentation. For each molecule, we generate k ground-truth conformers. During training, we randomly sample one conformer \mathbf{X}_0 and apply a random rigid transformation (translation and rotation) following [2, 29, 40]. This augmentation encourages D_θ to learn $SE(3)$ -invariant representations and mitigate overfitting, significantly improving performance.

Diffusion Transformer (DiT) Architecture. The network D_θ is a DiT [49] shown in Figure 2(b). Input atom tokens are formed by concatenating noisy coordinates \mathbf{X}_σ and atom types \mathbf{A} , followed by an MLP projection. The noise level σ is embedded using frequency encoding and an MLP. This noise embedding is added to the spectral embedding \mathbf{z}_S to form the conditioning vector, which is integrated into the DiT blocks via adaptive layer normalization (adaLN-Zero) [49].

Conditional Dropout and Classifier-Free Guidance. To improve robustness and flexibility in conditioning on different NMR spectra, we adopt classifier-free guidance (CFG) [19]. During training, the ^1H NMR spectrum is dropped with probability $p_H = 0.1$, the ^{13}C NMR spectrum is dropped with $p_C = 0.1$, and both are dropped simultaneously with $p_{\text{both}} = 0.1$. At inference, conditional and unconditional predictions are combined via

$$D_\theta^\omega(\mathbf{X}_\sigma; \sigma, \mathbf{A}, \mathbf{z}_S) = (1 + \omega) D_\theta(\mathbf{X}_\sigma; \sigma, \mathbf{A}, \mathbf{z}_S) - \omega D_\theta(\mathbf{X}_\sigma; \sigma, \mathbf{A}), \quad (6)$$

where $\omega \geq 0$ controls guidance scale. This enables generation conditioned on either or both spectra, improving versatility and performance. See Appendix A and D.2 for full training and sampling algorithms and hyperparameter settings.

4 Related Work

NMR Spectra Prediction. The forward task of predicting a given molecule’s NMR spectra is relatively established, facilitating data analysis and enabling the generation of simulated datasets for structure elucidation of simple compounds via database retrieval. These spectra prediction methods range from precise, computationally intensive quantum-chemical simulations to more recent exploratory ML approaches [6, 28, 13, 35, 31, 16, 39, 44]. Following established dataset curation practices [22, 4], we create our SpectraNP dataset using the commercial software MestReNova [44], which combines closed-source ML and chemoinformatics algorithms.

NMR Structure Elucidation. Structure elucidation from NMR spectroscopy is a challenging inverse problem, due to the complexity of spectra data and the vast size of chemical space [60, 17]. Traditional computer-aided systems, while historically employed and useful, often suffer from computational inefficiencies [8]. Recent ML methods have tackled this challenge, but most simplify the problem by predicting molecular substructures instead of full molecules [38, 36, 5, 64, 76, 33], or by leveraging richer inputs, such as additional experimental data beyond NMR [54, 12, 50, 55, 11, 9, 63, 53] and database retrieval [78, 62, 33]. In contrast, our method directly tackles the *de novo* elucidation of molecular structures using only raw 1D NMR spectra and chemical formulae.

De Novo Structure Elucidation from 1D NMR Spectra. Recent work developing machine learning methods for *de novo* structure elucidation from 1D NMR spectra focuses on structurally simple molecules, leveraging either chemical language models or graph-based models. Chemical language models [80, 22, 3, 4] generate SMILES strings [71], a sequence-based molecular representation. For example, Hu et al. [22] use a multitask transformer pre-trained on 3.1M substructure-molecule pairs and fine-tuned on 143k NMR spectra from SpectraBase [26], achieving 69.6% top-15 accuracy for molecules under 59 atoms. Alberts et al. [3, 4] employ transformers to predict SMILES from text-based 1D NMR peak lists and chemical formulas, reporting 89.98% top-10 accuracy on the USPTO dataset [41] for molecules under 101 atoms. Graph-based models iteratively construct molecular graphs with GNNs, using methods like Markov decision processes or Monte Carlo tree search [27, 23, 61]. However, these methods do not handle molecules with more than 64 atoms or large rings (>8 atoms), likely due to the limited availability of large-scale spectral datasets and the high computational cost of search-based algorithms for complex molecules. To the best of our knowledge, CHEFNMR is the first method based on 3D atomic diffusion models for NMR structure elucidation that scales to complex natural products.

3D Molecular Diffusion Models. Diffusion models have emerged as powerful tools for 3D molecular generation. E(3)-equivariant GNNs [74, 21, 75, 46] enforce geometric constraints, but non-equivariant transformers are increasingly favored for their scalability and performance in small molecule generation [69, 40, 29] and protein structure prediction [2, 15] involving hundreds of thousands of atoms. Inspired by these recent trends, we apply a scalable DiT [49] to generate 3D atomic structures from NMR spectra, exploiting their scalability and expressivity by creating a large synthetic NMR spectra dataset of natural products.

5 Experiments

5.1 Dataset Curation

Synthetic Datasets. We evaluate models on two public benchmarks, SpectraBase [22] and USPTO [4], and our self-curated SpectraNP dataset. SpectraBase contains simple molecules [22, 26], while USPTO features a broader range of molecules in chemical reactions [41]. SpectraNP combines data from NPAtlas [52], a database of small molecules from bacteria and fungi, with a subset of NP-MRD [72] including various natural products.

Table 1: Summary of dataset statistics.

Synthetic	# Molecules	# Atoms
SpectraBase [22]	141k	[3, 59]
USPTO [4]	745k	[8, 101]
SpectraNP	111k	[4, 274]
Experimental	# Molecules	# Solvents
SpecTeach [65]	238	2
NMRShiftDB2 [34]	23k	>7

Experimental Datasets. To evaluate the ability of models trained on synthetic data to generalize to experimental data, we curate two experimental datasets. Following [4], we include the SpecTeach dataset [65], which contains 238 simple molecules for spectroscopy education. We also include NMRShiftDB2 [34], a larger-scale dataset of ^{13}C NMR spectra in various solvents, following [61, 28]. These experimental datasets include impurities, solvents, and baseline noise (See Figure 5), enabling robustness testing for experimental variations.

Data Structure and Preprocessing. Each data entry is a tuple (*SMILES*, ^1H NMR spectrum, ^{13}C NMR spectrum, atom features). SMILES strings are canonicalized with stereochemistry removed, and synthetic spectra are simulated using MestreNova [44]. Atom features include atom types *A* and 3D conformations *X*, generated using RDKit’s ETKDgV3 algorithm [1] given the SMILES string.

To preprocess datasets, any duplicate SMILES are first removed. ^1H and ^{13}C spectra are interpolated to 10,000-dimensional vectors following [22, 4], and normalized by their highest peak intensity, except for SpectraBase [22] and experimental datasets, where ^{13}C spectra are binned into 80 binary vectors. To validate 3D conformers, SMILES strings are reconstructed from atom types and 3D coordinates using RDKit’s DetermineBonds function [1], and molecules failing reconstruction are discarded. See Appendix C for dataset curation details.

5.2 Experimental Setup

Baselines. We compare CHEFNMR against two existing chemical language models and introduce a graph-based model to assess the impact of molecular representations on the structure elucidation task.

The chemical language models are: (1) **Hu et al.** [22] propose a two-stage multitask transformer for predicting SMILES from 1D NMR spectra. Their method pre-defines 957 substructures and pre-trains a substructure-to-SMILES model on 3.1M molecules, and then fine-tunes a multitask transformer on 143k NMR spectra from SpectraBase. We retrain their substructure-to-SMILES model on the same 3.1M dataset and fine-tune it on each synthetic benchmark. (2) **Alberts et al.** [4] develop a transformer to predict stereochemical SMILES from text-based 1D NMR peak lists and chemical formulae. Due to unavailable inference code and differences in input (peak lists vs. raw spectra) and output (stereo vs. non-stereo SMILES), we report their published results on USPTO and SpecTeach.

To test an alternative graph-based representation, we also propose **NMR-DiGress**, a model integrating the discrete graph diffusion model DiGress [66] with our NMR-ConvFormer. Molecular graphs are represented as atom types \mathbf{A} and bond matrices $\mathbf{E} \in \{0, 1\}^{N \times N \times d_{\text{bond}}}$, where N is the number of atoms and d_{bond} is the number of bond types. DiGress adds noise to each atom or bond independently via discrete Markov chains, and trains a graph transformer to reverse this process to generate molecular graphs. We adapt DiGress to condition on spectral features from NMR-ConvFormer and atom types \mathbf{A} , generating only bond matrices. See Appendix B and D.1 for full algorithms and detailed settings.

CHEFNMR. We evaluate two variants: CHEFNMR-S (134M parameters) and CHEFNMR-L (462M parameters) with the same NMR-ConvFormer and different sizes of DiT. See Appendix D.2 for additional experimental details.

Metrics. We evaluate models using: (1) **Top- k matching accuracy**, which checks whether the ground truth SMILES string is exactly matched by any of the top- k predicted molecules. For non-language models, we reconstruct canonical, non-stereo SMILES from the predicted molecular graph (atom types and generated bond matrix) or 3D structure (atom types and generated 3D coordinates) using RDKit [1]. (2) **Top- k maximum Tanimoto similarity**, which evaluates structural similarity between the ground truth and the most similar molecule in the top- k predictions, using the Tanimoto similarity of Morgan fingerprints (length 2048, radius 2) [1].

6 Results

This section presents the quantitative and qualitative results across benchmarks. Section 6.1 shows CHEFNMR’s state-of-the-art performance on synthetic datasets, and Section 6.2 demonstrates robust zero-shot generalization on experimental datasets. Section 6.3 presents ablation studies on the contributions of the diffusion training process and the NMR-ConvFormer spectra embedder.

6.1 Performance on Synthetic Spectra

Table 2 summarizes the performance on synthetic ^1H and ^{13}C NMR spectra. CHEFNMR significantly surpasses all baselines in matching accuracy and maximum Tanimoto similarity across datasets. The

Table 2: Performance on synthetic ^1H and ^{13}C NMR spectra, reported as the mean \pm standard deviation over three independent sampling runs. Acc%: accuracy; Sim: Tanimoto similarity. *: reported results. N/A: not applicable.

Dataset	Model	Top-1		Top-5		Top-10	
		Acc% \uparrow	Sim \uparrow	Acc% \uparrow	Sim \uparrow	Acc% \uparrow	Sim \uparrow
SpectraBase	Hu et al.	45.24 \pm .18	0.686 \pm .001	62.37 \pm .08	0.815 \pm .001	67.38 \pm .05	0.847 \pm .001
	NMR-DiGress	43.56 \pm .30	0.625 \pm .002	62.47 \pm .20	0.779 \pm .002	68.39 \pm .35	0.817 \pm .001
	CHEFNMR-S	69.15 \pm .08	0.807 \pm .002	82.09 \pm .24	0.904 \pm .002	85.30 \pm .04	0.922 \pm .000
	CHEFNMR-L	72.04\pm.02	0.833\pm.000	85.24\pm.10	0.923\pm.001	88.20\pm.07	0.940\pm.000
USPTO	Hu et al.	38.02 \pm .02	0.674 \pm .001	55.85 \pm .04	0.810 \pm .000	61.76 \pm .03	0.845 \pm .000
	Alberts et al.*	73.38 \pm .08	N/A	87.94 \pm .14	N/A	89.98 \pm .16	N/A
	NMR-DiGress	22.51 \pm .13	0.504 \pm .000	41.26 \pm .12	0.708 \pm .001	48.87 \pm .11	0.761 \pm .000
	CHEFNMR-S	81.16 \pm .08	0.902 \pm .000	91.03 \pm .05	0.964 \pm .000	92.90 \pm .05	0.973\pm.000
	CHEFNMR-L	81.57\pm.09	0.912\pm.000	91.09\pm.11	0.965\pm.000	93.01\pm.05	0.973\pm.000
SpectraNP	Hu et al.	19.26 \pm .10	0.585 \pm .001	34.00 \pm .19	0.736 \pm .001	39.87 \pm .02	0.774 \pm .001
	NMR-DiGress	2.12 \pm .14	0.260 \pm .001	6.31 \pm .08	0.432 \pm .001	9.17 \pm .11	0.485 \pm .000
	CHEFNMR-S	40.37\pm.33	0.583 \pm .004	59.08 \pm .28	0.791 \pm .000	64.37 \pm .08	0.834 \pm .001
	CHEFNMR-L	40.15 \pm .29	0.631\pm.004	59.83\pm.30	0.822\pm.002	65.74\pm.09	0.860\pm.000

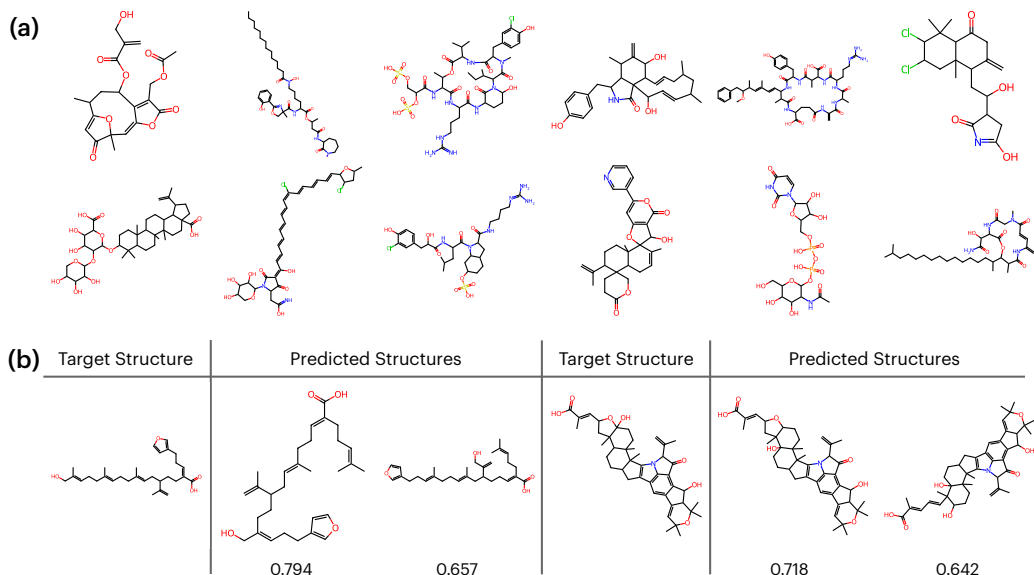


Figure 3: Examples of CHEFNMR’s predictions on the synthetic SpectraNP dataset. **(a)** Correctly predicted diverse and complex natural products in top-1 predictions. **(b)** Incorrect top-2 predictions ranked by Tanimoto similarity remain chemically valid and structurally similar to the ground truth.

advantage is most pronounced on the challenging SpectraNP dataset, where CHEFNMR achieves 40% top-1 accuracy compared to 19% for Hu et al. and only 2% for NMR-DiGress.

Performance scales up with both model and dataset size. CHEFNMR-S outperforms baselines by large margins across all datasets, and CHEFNMR-L further improves accuracy. Larger datasets also yield better results, with the highest performance observed on USPTO (745k data), followed by SpectraBase (141k data) and SpectraNP (111k data). This suggests expanding SpectraNP could further enhance performance in elucidating complex natural products.

Figure 3 provides qualitative examples of CHEFNMR’s performance on SpectraNP. CHEFNMR accurately predicts diverse and complex natural product structures in its top-1 predictions (Figure 3(a)). We additionally show incorrect predictions (Figure 3(b)), and find that many of the generated structures remain chemically valid and similar to the ground truth. Additional qualitative examples are provided in Appendix F.4.

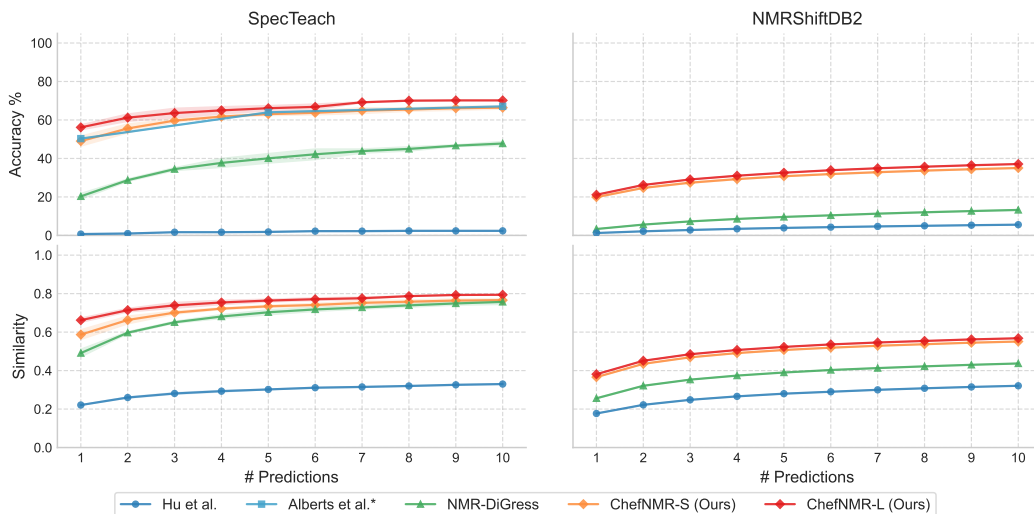


Figure 4: Zero-shot performance on experimental NMR spectra, shown as the mean \pm standard deviation over three independent sampling runs. Models are trained on USPTO. Evaluation is on ^1H and ^{13}C spectra for SpecTeach, and on ^{13}C spectra for NMRShiftDB2. *: reported results.

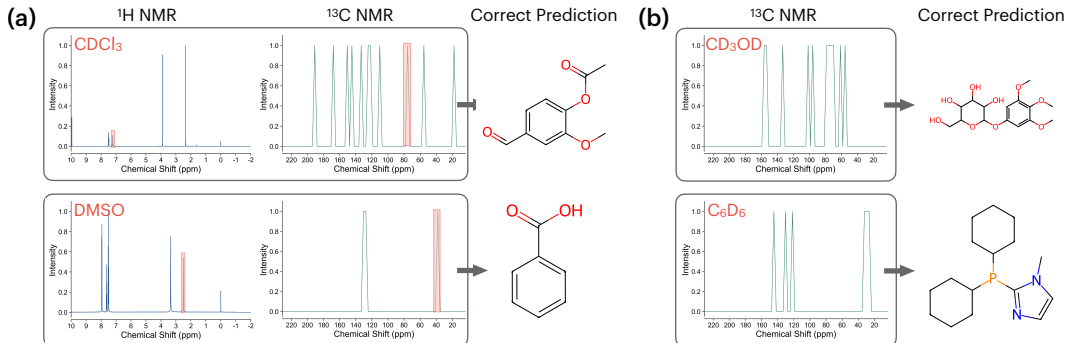


Figure 5: Examples of correct structures in CHEFNMR’s top-1 predictions on experimental (a) SpecTeach and (b) NMRShiftDB2 datasets respectively, with solvent peaks marked in red.

6.2 Zero-shot Performance on Experimental Spectra

Figure 4 reports the zero-shot performance on experimental ^1H and ^{13}C NMR spectra. CHEFNMR achieves 56% top-1 accuracy on SpecTeach and 21% on NMRShiftDB2, significantly outperforming Hu et al. [22] and NMR-DiGress, which generalize poorly to both experimental benchmarks. Figure 5 shows that CHEFNMR can generate the correct structures in its top-1 predictions despite substantial experimental variations, such as solvent effect and impurities.

6.3 Ablation Studies

We perform extensive ablation studies to assess the contributions of key components in diffusion training and the NMR-ConvFormer on the SpectraBase dataset. Each row in Table 3 corresponds to a variant with one component removed or modified from the base setting. Coordinate augmentation improves accuracy by 20%, indicating learning symmetries is crucial. Within the NMR-ConvFormer, convolutional tokenizer, MAP pooling, and dropout are relatively important. Detailed settings and additional ablations, including separate contributions of ^1H and ^{13}C spectra, are provided in Appendix E.

Table 3: Ablation results (Top-1 Acc% / Sim).

Configuration	Acc@1% \uparrow	Sim@1 \uparrow
Base (CHEFNMR-S)	69.15	0.807
<i>Diffusion Training Ablation</i>		
– Coord Augmentation	49.75	0.651
– Smooth LDDT Loss	68.31	0.798
<i>NMR-ConvFormer Ablation</i>		
– Conv Tokenizer	61.78	0.756
– Token Count Reduction	66.28	0.789
– Transformer Block	68.12	0.797
– MAP Pooling	62.97	0.758
– Dropout	65.48	0.777

7 Conclusion

In this work, we address the challenge of determining structures for complex natural products directly from raw 1D NMR spectra and chemical formulas. We introduce CHEFNMR, an end-to-end diffusion model that combines a hybrid convolutional transformer for spectral encoding with a Diffusion Transformer for 3D molecular structure generation. To encompass the chemical diversity present in natural products, we curate SpectraNP, a large-scale dataset of synthetic 1D NMR spectra for natural products. Our approach achieves state-of-the-art accuracy on synthetic and experimental benchmarks, with ablation studies validating the importance of key design components.

Several limitations highlight promising directions for future work. Expanding the training set to include experimental spectra and more natural products could further improve model performance. Additional information, such as 2D NMR spectra, could be incorporated to resolve stereochemistry. Furthermore, adding a confidence module could help chemists better assess the reliability of predicted structures. Overall, automating NMR-based structure elucidation has the potential to significantly accelerate molecular discovery. Careful validation and responsible deployment will be essential to ensure safe and impactful use in real-world applications.

Acknowledgements

The authors acknowledge the use of computing resources at Princeton Research Computing, a consortium of groups led by the Princeton Institute for Computational Science and Engineering (PICSciE) and Office of Information Technology’s Research Computing. The Zhong lab is grateful for support from the Princeton Catalysis Initiative, Princeton School of Engineering and Applied Sciences, Chan Zuckerberg Imaging Institute, Janssen Pharmaceuticals, and Generate Biomedicines. The Seyedsayamdost lab is grateful for support from the Princeton Catalysis Initiative and a Princeton SEAS grant. The funders had no role in study design, data collection and analysis, decision to publish or preparation of the manuscript. The silhouette of *Actinomyces* used in Figure 1 was created by Matt Crook and licensed under CC BY-SA 3.0 Unported.

References

- [1] RDKit: Open-source cheminformatics. <https://www.rdkit.org/>.
- [2] Josh Abramson, Jonas Adler, Jack Dunger, Richard Evans, Tim Green, Alexander Pritzel, Olaf Ronneberger, Lindsay Willmore, Andrew J Ballard, Joshua Bambrick, et al. Accurate structure prediction of biomolecular interactions with alphafold 3. *Nature*, 630(8016):493–500, 2024.
- [3] Marvin Alberts, Federico Zipoli, and Alain Vaucher. Learning the language of nmr: structure elucidation from nmr spectra using transformer models. In *AI for Accelerated Materials Design-NeurIPS 2023 Workshop*, 2023.
- [4] Marvin Alberts, Oliver Schilter, Federico Zipoli, Nina Hartrampf, and Teodoro Laino. Unraveling molecular structure: A multimodal spectroscopic dataset for chemistry. *Advances in Neural Information Processing Systems*, 37:125780–125808, 2024.
- [5] Josef Berman, Yehudit Aperstein, and Abraham Yosipof. Elucidation of molecular substructures from nuclear magnetic resonance spectra using gradient boosting. In *International Conference on Artificial Neural Networks*, pages 31–42. Springer, 2024.
- [6] Yuri Binev, Maria MB Marques, and João Aires-de Sousa. Prediction of 1h nmr coupling constants with associative neural networks trained for chemical shifts. *Journal of Chemical Information and Modeling*, 47(6):2089–2097, 2007.
- [7] Sebastian Böcker and Kai Dührkop. Fragmentation trees reloaded. *Journal of Cheminformatics*, 8:1–26, 2016.
- [8] Darcy C Burns, Eugene P Mazzola, and William F Reynolds. The role of computer-assisted structure elucidation (case) programs in the structure elucidation of complex natural products. *Natural Product Reports*, 36(6):919–933, 2019.
- [9] Edwin Chacko, Rudra Sondhi, Arnav Praveen, Kylie L Luska, and Rodrigo Vargas-Hernandez. Spectro: A multi-modal approach for molecule elucidation using ir and nmr data. In *AI for Accelerated Materials Design-NeurIPS 2024*, 2024.
- [10] Gabriele Corso, Hannes Stärk, Bowen Jing, Regina Barzilay, and Tommi Jaakkola. Diffdock: Diffusion steps, twists, and turns for molecular docking. *arXiv preprint arXiv:2210.01776*, 2022.
- [11] Sriram Devata, Bhuvanesh Sridharan, Sarvesh Mehta, Yashaswi Pathak, Siddhartha Laghuvarapu, Girish Varma, and U Deva Priyakumar. Deepspinn—deep reinforcement learning for molecular structure prediction from infrared and 13 c nmr spectra. *Digital Discovery*, 3(4): 818–829, 2024.
- [12] Susanna Di Vita, Florian Grötschla, Luca A Lanzendörfer, and Roger Wattenhofer. Leveraging pre-trained lms for rapid and accurate structure elucidation from 2d nmr data. In *AI for Accelerated Materials Design Workshop (AI4Mat@ NeurIPS)*, 2024.
- [13] Peng Gao, Jun Zhang, Qian Peng, Jie Zhang, and Vassiliki-Alexandra Glezakou. General protocol for the accurate prediction of molecular 13c/1h nmr chemical shifts via machine learning augmented dft. *Journal of Chemical Information and Modeling*, 60(8):3746–3754, 2020.

- [14] Susana P Gaudêncio, Engin Bayram, Lada Lukić Bilela, Mercedes Cueto, Ana R Díaz-Marrero, Berat Z Haznedaroglu, Carlos Jimenez, Manolis Mandalakis, Florbela Pereira, Fernando Reyes, et al. Advanced methods for natural products discovery: bioactivity screening, dereplication, metabolomics profiling, genomic sequencing, databases and informatic tools, and structure elucidation. *Marine Drugs*, 21(5):308, 2023.
- [15] Tomas Geffner, Kieran Didi, Zuobai Zhang, Danny Reidenbach, Zhonglin Cao, Jason Yim, Mario Geiger, Christian Dallago, Emine Kucukbenli, Arash Vahdat, et al. Proteina: Scaling flow-based protein structure generative models. *arXiv preprint arXiv:2503.00710*, 2025.
- [16] Yanfei Guan, SV Shree Sowndarya, Liliana C Gallegos, Peter C St John, and Robert S Paton. Real-time prediction of 1 h and 13 c chemical shifts with dft accuracy using a 3d graph neural network. *Chemical Science*, 12(36):12012–12026, 2021.
- [17] Kehan Guo, Yili Shen, Gisela Abigail Gonzalez-Montiel, Yue Huang, Yujun Zhou, Mihir Surve, Zhichun Guo, Prayel Das, Nitesh V Chawla, Olaf Wiest, et al. Artificial intelligence in spectroscopy: Advancing chemistry from prediction to generation and beyond. *arXiv preprint arXiv:2502.09897*, 2025.
- [18] Lichun He, Bin Jiang, Yun Peng, Xu Zhang, and Maili Liu. Nmr based methods for metabolites analysis. *Analytical Chemistry*, 97(10):5393–5406, 2025.
- [19] Jonathan Ho and Tim Salimans. Classifier-free diffusion guidance. *arXiv preprint arXiv:2207.12598*, 2022.
- [20] Jonathan Ho, Ajay Jain, and Pieter Abbeel. Denoising diffusion probabilistic models. *Advances in Neural Information Processing Systems*, 33:6840–6851, 2020.
- [21] Emiel Hoogeboom, Victor Garcia Satorras, Clément Vignac, and Max Welling. Equivariant diffusion for molecule generation in 3d. In *International Conference on Machine Learning*, pages 8867–8887. PMLR, 2022.
- [22] Frank Hu, Michael S Chen, Grant M Rotskoff, Matthew W Kanan, and Thomas E Markland. Accurate and efficient structure elucidation from routine one-dimensional nmr spectra using multitask machine learning. *ACS Central Science*, 10(11):2162–2170, 2024.
- [23] Zhaorui Huang, Michael S Chen, Cristian P Woroch, Thomas E Markland, and Matthew W Kanan. A framework for automated structure elucidation from routine nmr spectra. *Chemical Science*, 12(46):15329–15338, 2021.
- [24] Aapo Hyvärinen and Peter Dayan. Estimation of non-normalized statistical models by score matching. *Journal of Machine Learning Research*, 6(4), 2005.
- [25] John B Ingraham, Max Baranov, Zak Costello, Karl W Barber, Wujie Wang, Ahmed Ismail, Vincent Frappier, Dana M Lord, Christopher Ng-Thow-Hing, Erik R Van Vlack, et al. Illuminating protein space with a programmable generative model. *Nature*, 623(7989):1070–1078, 2023.
- [26] John Wiley & Sons, Inc. Spectrabase: Online spectral database. <https://spectrabase.com/>.
- [27] Eric Jonas. Deep imitation learning for molecular inverse problems. *Advances in Neural Information Processing Systems*, 32, 2019.
- [28] Eric Jonas and Stefan Kuhn. Rapid prediction of nmr spectral properties with quantified uncertainty. *Journal of Cheminformatics*, 11:1–7, 2019.
- [29] Chaitanya K Joshi, Xiang Fu, Yi-Lun Liao, Vahe Gharakhanyan, Benjamin Kurt Miller, Anuroop Sriram, and Zachary W Ulissi. All-atom diffusion transformers: Unified generative modelling of molecules and materials. *arXiv preprint arXiv:2503.03965*, 2025.
- [30] John Jumper, Richard Evans, Alexander Pritzel, Tim Green, Michael Figurnov, Olaf Ronneberger, Kathryn Tunyasuvunakool, Russ Bates, Augustin Žídek, Anna Potapenko, et al. Highly accurate protein structure prediction with alphafold. *Nature*, 596(7873):583–589, 2021.

- [31] Seokho Kang, Youngchun Kwon, Dongseon Lee, and Youn-Suk Choi. Predictive modeling of nmr chemical shifts without using atomic-level annotations. *Journal of Chemical Information and Modeling*, 60(8):3765–3769, 2020.
- [32] Tero Karras, Miika Aittala, Timo Aila, and Samuli Laine. Elucidating the design space of diffusion-based generative models. *Advances in Neural Information Processing Systems*, 35: 26565–26577, 2022.
- [33] Hyun Woo Kim, Chen Zhang, Raphael Reher, Mingxun Wang, Kelsey L Alexander, Louis-Félix Nothias, Yoo Kyong Han, Hyeji Shin, Ki Yong Lee, Kyu Hyeong Lee, et al. Deepsat: Learning molecular structures from nuclear magnetic resonance data. *Journal of Cheminformatics*, 15(1): 71, 2023.
- [34] Stefan Kuhn and Nils E Schlörer. Facilitating quality control for spectra assignments of small organic molecules: nmrshiftdb2—a free in-house nmr database with integrated lims for academic service laboratories. *Magnetic Resonance in Chemistry*, 53(8):582–589, 2015.
- [35] Youngchun Kwon, Dongseon Lee, Youn-Suk Choi, Myeonginn Kang, and Seokho Kang. Neural message passing for nmr chemical shift prediction. *Journal of Chemical Information and Modeling*, 60(4):2024–2030, 2020.
- [36] Gwanho Lee, Hyekyoung Shim, Juhyun Cho, and Sang-Il Choi. Machine-learning approach to identify organic functional groups from ft-ir and nmr spectral data. *ACS Omega*, 2025.
- [37] Juho Lee, Yoonho Lee, Jungtaek Kim, Adam Kosiorek, Seungjin Choi, and Yee Whye Teh. Set transformer: A framework for attention-based permutation-invariant neural networks. In *International Conference on Machine Learning*, pages 3744–3753. PMLR, 2019.
- [38] Chongcan Li, Yong Cong, and Weihua Deng. Identifying molecular functional groups of organic compounds by deep learning of nmr data. *Magnetic Resonance in Chemistry*, 60(11): 1061–1069, 2022.
- [39] Jie Li, Jiashu Liang, Zhe Wang, Aleksandra L Ptaszek, Xiao Liu, Brad Ganoe, Martin Head-Gordon, and Teresa Head-Gordon. Highly accurate prediction of nmr chemical shifts from low-level quantum mechanics calculations using machine learning. *Journal of Chemical Theory and Computation*, 20(5):2152–2166, 2024.
- [40] Zhiyuan Liu, Yanchen Luo, Han Huang, Enzhi Zhang, Sihang Li, Junfeng Fang, Yaorui Shi, Xiang Wang, Kenji Kawaguchi, and Tat-Seng Chua. Next-mol: 3d diffusion meets 1d language modeling for 3d molecule generation. *arXiv preprint arXiv:2502.12638*, 2025.
- [41] Daniel Mark Lowe. *Extraction of chemical structures and reactions from the literature*. PhD thesis, 2012.
- [42] Xin-Yu Lu, Hao-Ping Wu, Hao Ma, Hui Li, Jia Li, Yan-Ti Liu, Zheng-Yan Pan, Yi Xie, Lei Wang, Bin Ren, et al. Deep learning-assisted spectrum–structure correlation: state-of-the-art and perspectives. *Analytical Chemistry*, 96(20):7959–7975, 2024.
- [43] Valerio Mariani, Marco Biasini, Alessandro Barbato, and Torsten Schwede. lddt: a local superposition-free score for comparing protein structures and models using distance difference tests. *Bioinformatics*, 29(21):2722–2728, 2013.
- [44] Mestrelab Research. mnova: Nmr data processing and analysis software. <https://mestrelab.com/main-product/mnova>.
- [45] Adrian Mirza and Kevin Maik Jablonka. Elucidating structures from spectra using multimodal embeddings and discrete optimization. 2024.
- [46] Alex Morehead and Jianlin Cheng. Geometry-complete diffusion for 3d molecule generation and optimization. *Communications Chemistry*, 7(1):150, 2024.
- [47] Michael W Mullowney, Katherine R Duncan, Somayah S Elsayed, Neha Garg, Justin JJ van der Hoof, Nathaniel I Martin, David Meijer, Barbara R Terlouw, Friederike Biermann, Kai Blin, et al. Artificial intelligence for natural product drug discovery. *Nature Reviews Drug Discovery*, 22(11):895–916, 2023.

- [48] David J Newman and Gordon M Cragg. Natural products as sources of new drugs over the nearly four decades from 01/1981 to 09/2019. *Journal of Natural Products*, 83(3):770–803, 2020.
- [49] William Peebles and Saining Xie. Scalable diffusion models with transformers. In *Proceedings of the IEEE/CVF International Conference on Computer Vision*, pages 4195–4205, 2023.
- [50] Matevž Pesek, Andraž Juvan, Jure Jakoš, Janez Košmrlj, Matija Marolt, and Martin Gazvoda. Database independent automated structure elucidation of organic molecules based on ir, ¹h nmr, ¹³c nmr, and ms data. *Journal of Chemical Information and Modeling*, 61(2):756–763, 2020.
- [51] Daniil Polykovskiy, Alexander Zhebrak, Benjamin Sanchez-Lengeling, Sergey Golovanov, Oktai Tatanov, Stanislav Belyaev, Rauf Kurbanov, Aleksey Artamonov, Vladimir Aladinskiy, Mark Veselov, et al. Molecular sets (moses): a benchmarking platform for molecular generation models. *Frontiers in Pharmacology*, 11:565644, 2020.
- [52] Ella F Poynton, Jeffrey A van Santen, Matthew Pin, Marla Macias Contreras, Emily McMann, Jonathan Parra, Brandon Showalter, Liana Zaroubi, Katherine R Duncan, and Roger G Linington. The natural products atlas 3.0: extending the database of microbially derived natural products. *Nucleic Acids Research*, 53(D1):D691–D699, 2025.
- [53] Martin Priessner, Richard Lewis, Jon Paul Janet, Isak Lemurell, Magnus Johansson, Jonathan Goodman, and Anna Tomberg. Enhancing molecular structure elucidation: Multimodaltransformer for both simulated and experimental spectra. 2024.
- [54] Raphael Reher, Hyun Woo Kim, Chen Zhang, Huanru Henry Mao, Mingxun Wang, Louis-Félix Nothias, Andres Mauricio Caraballo-Rodriguez, Evgenia Glukhov, Bahar Teke, Tiago Leao, et al. A convolutional neural network-based approach for the rapid annotation of molecularly diverse natural products. *Journal of the American Chemical Society*, 142(9):4114–4120, 2020.
- [55] J Benji Rowlands, Lina Jonsson, Jonathan Goodman, Peter Howe, Werngard Czechtizky, Tomas Leek, and Richard James Lewis. Towards automatically verifying chemical structures: the powerful combination of 1 h nmr and ir spectroscopy. *Chemical Science*, 2025.
- [56] Vinodh J Sahayasheela, Manendra B Lankadasari, Vipin Mohan Dan, Syed G Dastager, Ganesh N Pandian, and Hiroshi Sugiyama. Artificial intelligence in microbial natural product drug discovery: current and emerging role. *Natural Product Reports*, 39(12):2215–2230, 2022.
- [57] Arne Schneuing, Charles Harris, Yuanqi Du, Kieran Didi, Arian Jamasb, Ilia Igashov, Weitao Du, Carla Gomes, Tom L Blundell, Pietro Lio, et al. Structure-based drug design with equivariant diffusion models. *Nature Computational Science*, 4(12):899–909, 2024.
- [58] Kaushik Seshadri, Abner ND Abad, Kyle K Nagasawa, Karl M Yost, Colin W Johnson, Moriel J Dror, and Yi Tang. Synthetic biology in natural product biosynthesis. *Chemical Reviews*, 2025.
- [59] Yang Song, Jascha Sohl-Dickstein, Diederik P Kingma, Abhishek Kumar, Stefano Ermon, and Ben Poole. Score-based generative modeling through stochastic differential equations. *arXiv preprint arXiv:2011.13456*, 2020.
- [60] Bhuvanesh Sridharan, Manan Goel, and U Deva Priyakumar. Modern machine learning for tackling inverse problems in chemistry: molecular design to realization. *Chemical Communications*, 58(35):5316–5331, 2022.
- [61] Bhuvanesh Sridharan, Sarvesh Mehta, Yashaswi Pathak, and U Deva Priyakumar. Deep reinforcement learning for molecular inverse problem of nuclear magnetic resonance spectra to molecular structure. *The Journal of Physical Chemistry Letters*, 13(22):4924–4933, 2022.
- [62] Hanyu Sun, Xi Xue, Xue Liu, Hai-Yu Hu, Yafeng Deng, and Xiaojian Wang. Cross-modal retrieval between ¹³c nmr spectra and structures based on focused libraries. *Analytical Chemistry*, 96(15):5763–5770, 2024.
- [63] Xiaofeng Tan. A transformer based generative chemical language ai model for structural elucidation of organic compounds. *Journal of Cheminformatics*, 17(1):103, 2025.

- [64] ZiJing Tian, Yan Dai, Feng Hu, ZiHao Shen, HongLing Xu, HongWen Zhang, JinHang Xu, YuTing Hu, YanYan Diao, and HongLin Li. Enhancing chemical reaction monitoring with a deep learning model for nmr spectra image matching to target compounds. *Journal of Chemical Information and Modeling*, 64(14):5624–5633, 2024.
- [65] Scott E Van Bramer and Loyd D Bastin. Spectroscopy data for undergraduate teaching. *Journal of Chemical Education*, 100(10):3897–3902, 2023.
- [66] Clement Vignac, Igor Krawczuk, Antoine Siraudin, Bohan Wang, Volkan Cevher, and Pascal Frossard. Digress: Discrete denoising diffusion for graph generation. *arXiv preprint arXiv:2209.14734*, 2022.
- [67] Liang Wang, Shaozhen Liu, Yu Rong, Deli Zhao, Qiang Liu, and Shu Wu. Molspectra: Pre-training 3d molecular representation with multi-modal energy spectra. *arXiv preprint arXiv:2502.16284*, 2025.
- [68] Yixin Wang, Fan Wang, Wenxiu Liu, Yifei Geng, Yahong Shi, Yu Tian, Bin Zhang, Yun Luo, and Xiaobo Sun. New drug discovery and development from natural products: Advances and strategies. *Pharmacology & Therapeutics*, page 108752, 2024.
- [69] Yuyang Wang, Ahmed A Elhag, Navdeep Jaitly, Joshua M Susskind, and Miguel Angel Bautista. Swallowing the bitter pill: Simplified scalable conformer generation. *arXiv preprint arXiv:2311.17932*, 2023.
- [70] Joseph L Watson, David Juergens, Nathaniel R Bennett, Brian L Trippe, Jason Yim, Helen E Eisenach, Woody Ahern, Andrew J Borst, Robert J Ragotte, Lukas F Milles, et al. De novo design of protein structure and function with rdiffusion. *Nature*, 620(7976):1089–1100, 2023.
- [71] David Weininger. Smiles, a chemical language and information system. 1. introduction to methodology and encoding rules. *Journal of Chemical Information and Computer Sciences*, 28(1):31–36, 1988.
- [72] David S Wishart, Tanvir Sajed, Matthew Pin, Ella F Poynton, Bharat Goel, Brian L Lee, An Chi Guo, Sukanta Saha, Zinat Sayeeda, Scott Han, et al. The natural products magnetic resonance database (np-mrd) for 2025. *Nucleic Acids Research*, 53(D1):D700–D708, 2025.
- [73] Jeremy Wohlwend, Gabriele Corso, Saro Passaro, Mateo Reveiz, Ken Leidal, Wojtek Swiderski, Tally Portnoi, Itamar Chinn, Jacob Silterra, Tommi Jaakkola, et al. Boltz-1: Democratizing biomolecular interaction modeling. *bioRxiv*, pages 2024–11, 2024.
- [74] Minkai Xu, Lantao Yu, Yang Song, Chence Shi, Stefano Ermon, and Jian Tang. Geodiff: A geometric diffusion model for molecular conformation generation. *arXiv preprint arXiv:2203.02923*, 2022.
- [75] Minkai Xu, Alexander S Powers, Ron O Dror, Stefano Ermon, and Jure Leskovec. Geometric latent diffusion models for 3d molecule generation. In *International Conference on Machine Learning*, pages 38592–38610. PMLR, 2023.
- [76] Wangdong Xu. Spectre: A spectral transformer for molecule identification. Master’s thesis, University of California, San Diego, 2025.
- [77] Xi Xue, Hanyu Sun, Minjian Yang, Xue Liu, Hai-Yu Hu, Yafeng Deng, and Xiaojian Wang. Advances in the application of artificial intelligence-based spectral data interpretation: a perspective. *Analytical Chemistry*, 95(37):13733–13745, 2023.
- [78] Zhuo Yang, Jianfei Song, Minjian Yang, Lin Yao, Jiahua Zhang, Hui Shi, Xiangyang Ji, Yafeng Deng, and Xiaojian Wang. Cross-modal retrieval between ¹³c nmr spectra and structures for compound identification using deep contrastive learning. *Analytical Chemistry*, 93(50):16947–16955, 2021.
- [79] Xiaohua Zhai, Alexander Kolesnikov, Neil Houlsby, and Lucas Beyer. Scaling vision transformers. In *Proceedings of the IEEE/CVF Conference on Computer Vision and Pattern Recognition*, pages 12104–12113, 2022.

- [80] Jinzhe Zhang, Kei Terayama, Masato Sumita, Kazuki Yoshizoe, Kengo Ito, Jun Kikuchi, and Koji Tsuda. Nmr-ts: de novo molecule identification from nmr spectra. *Science and Technology of Advanced Materials*, 21(1):552–561, 2020.

A Details of Conditional 3D Atomic Diffusion Model

In this section, we provide full training and sampling algorithms for the conditional 3D atomic diffusion model described in Section 3.2 of the main paper.

Training Procedure. The complete training procedure is outlined in Algorithm 1. The smooth LDDT loss is detailed in Algorithm 2, adapted from AlphaFold3 [2]. Unlike the original, which computes the smooth LDDT loss within a certain radius for proteins [2], we compute it of all atom pairs for small molecules, as small molecules are more compact in 3D space than proteins.

Algorithm 1 Diffusion Training.

```

1: procedure TRAINDIFFUSION( $D_\theta$ , atom types  $\mathbf{A}$ , ground-truth conformers  $\{\mathbf{X}^*\}_{k=1}^{K=3}$ , NMR spectra
    $\mathcal{S} = (\mathbf{s}_H, \mathbf{s}_C)$ , noise schedule  $(P_{\text{mean}}, P_{\text{std}}) = (-1.2, 1.3)$ , standard deviation of atom coordinates  $\sigma_{\text{data}}$ )
2:    $\mathcal{S} \leftarrow (\mathbf{s}_H, \mathbf{0}), (\mathbf{0}, \mathbf{s}_C)$ , or  $(\mathbf{0}, \mathbf{0})$  with probability 0.1 each ▷ Randomly drop spectra
3:    $\mathbf{z}_S \leftarrow \text{NMR-CONVFORMER}(\mathcal{S})$  ▷ Encode spectra
4:   sample  $k \sim \text{Uniform}(\{1, \dots, K\})$ ;  $\mathbf{X}_0 \leftarrow \mathbf{X}_k^*$  ▷ Select a target conformer
5:    $\mathbf{X}_0 \leftarrow \mathbf{X}_0 - \bar{\mathbf{X}}_0$  ▷ Center coordinates
6:   sample  $\mathbf{R} \sim \text{SO}(3)$ ,  $\mathbf{t} \sim \mathcal{N}(\mathbf{0}, \mathbf{I})$ ;  $\mathbf{X}_0 \leftarrow \mathbf{R}\mathbf{X}_0 + \mathbf{t}$  ▷ Random rigid transformation
7:   sample  $\ln \sigma \sim \mathcal{N}(P_{\text{mean}}, P_{\text{std}}^2)$ ;  $\sigma \leftarrow \sigma \cdot \sigma_{\text{data}}$  ▷ Sample noise scale
8:   sample  $\mathbf{n} \sim \mathcal{N}(\mathbf{0}, \sigma^2 \mathbf{I})$ ;  $\mathbf{X}_\sigma \leftarrow \mathbf{X}_0 + \mathbf{n}$  ▷ Add Gaussian noise
9:    $\hat{\mathbf{X}}_0 \leftarrow D_\theta(\mathbf{X}_\sigma; \sigma, \mathbf{A}, \mathbf{z}_S)$  ▷ Predict clean coordinates
10:  minimize  $\mathcal{L}_{\text{diffusion}} = \lambda(\sigma) \|\hat{\mathbf{X}}_0 - \mathbf{X}_0\|_2^2 + \mathcal{L}_{\text{smooth-lddt}}(\hat{\mathbf{X}}_0, \mathbf{X}_0)$ 
11: end procedure

```

Algorithm 2 Smooth LDDT Loss.

```

1: procedure SMOOTHLDDTLOSS(predicted coordinates  $\hat{\mathbf{X}}_0$ , ground-truth coordinates  $\mathbf{X}_0$ , thresholds
    $t = \{0.5, 1.0, 2.0, 4.0\}$ )
2:    $\hat{d}_{ij} \leftarrow \|\hat{\mathbf{x}}_i - \hat{\mathbf{x}}_j\|_2$ 
3:    $d_{ij} \leftarrow \|\mathbf{x}_{0,i} - \mathbf{x}_{0,j}\|_2$  ▷ Compute pairwise distances
4:    $\Delta d_{ij} \leftarrow |\hat{d}_{ij} - d_{ij}|$  ▷ Distance differences
5:    $\epsilon_{ij} \leftarrow \frac{1}{4} \sum_{k=1}^4 \text{sigmoid}(t_k - \Delta d_{ij})$  ▷ Preserved scores
6:    $\text{LDDT} \leftarrow \text{mean}_{i \neq j}(\epsilon_{ij})$  ▷ Mean score, excluding self-pairs
7:    $\mathcal{L}_{\text{smooth\_lddt}} \leftarrow 1 - \text{LDDT}$  ▷ Smooth LDDT loss
8:   return  $\mathcal{L}_{\text{smooth\_lddt}}$ 
9: end procedure

```

Preconditioning. To stabilize training across different noise levels, we precondition the denoising network D_θ following EDM [32]:

$$D_\theta(\mathbf{X}_\sigma; \sigma, \mathbf{A}, \mathbf{z}_S) = c_{\text{skip}}(\sigma) \mathbf{X}_\sigma + c_{\text{out}}(\sigma) F_\theta(c_{\text{in}}(\sigma) \mathbf{X}_\sigma; c_{\text{noise}}(\sigma), \mathbf{A}, \mathbf{z}_S), \quad (7)$$

where F_θ is the core neural network performing the actual computation. The scaling functions c_{skip} , c_{out} , c_{in} , c_{noise} , and the loss weight $\lambda(\sigma)$ are defined as EDM [32]:

$$c_{\text{skip}}(\sigma) = \frac{\sigma_{\text{data}}^2}{\sigma^2 + \sigma_{\text{data}}^2}, \quad c_{\text{out}}(\sigma) = \frac{\sigma \cdot \sigma_{\text{data}}}{\sqrt{\sigma_{\text{data}}^2 + \sigma^2}}, \quad (8)$$

$$c_{\text{in}}(\sigma) = \frac{1}{\sqrt{\sigma^2 + \sigma_{\text{data}}^2}}, \quad c_{\text{noise}}(\sigma) = \frac{1}{4} \ln(\sigma), \quad \lambda(\sigma) = \frac{\sigma^2 + \sigma_{\text{data}}^2}{(\sigma \cdot \sigma_{\text{data}})^2}. \quad (9)$$

Here, σ_{data} represents the standard deviation of atom coordinates in the dataset (see Appendix Table 7).

Conditional Dropout and Classifier-Free Guidance. To improve robustness and flexibility in conditioning on NMR spectra, we adopt classifier-free guidance (CFG) [19]. During training, the ^1H NMR spectrum is replaced with zeros with probability $p_H = 0.1$, the ^{13}C NMR spectrum is dropped with $p_C = 0.1$, and both are dropped simultaneously with $p_{\text{both}} = 0.1$ (see Algorithm 1). At inference, conditional and unconditional predictions are combined via

$$D_\theta^\omega(\mathbf{X}_\sigma; \sigma, \mathbf{A}, \mathbf{z}_S) = (1 + \omega) D_\theta(\mathbf{X}_\sigma; \sigma, \mathbf{A}, \mathbf{z}_S) - \omega D_\theta(\mathbf{X}_\sigma; \sigma, \mathbf{A}), \quad (10)$$

where $\omega \geq 0$ controls guidance scale. This enables generation conditioned on either or both spectra, improving versatility and performance. In this paper, we set $\omega \in \{1, 1.5, 2\}$ depending on datasets.

Algorithm 3 Diffusion Sampling using Stochastic Heun’s 2nd order Method.

```
1: procedure SAMPLEDIFFUSION( $D_\theta^\omega(\mathbf{X}_\sigma; \sigma, \mathbf{A}, \mathbf{z}_S)$ , atom type  $\mathbf{A}$ , NMR spectra embedding  $\mathbf{z}_S$ , noise  
   level schedule  $\sigma_{i \in \{0, \dots, N\}}$ ,  $\gamma_0 = 0.8$ ,  $\gamma_{\min} = 1.0$ ,  $\omega$  guidance scale)  
2:   sample  $\mathbf{X}_0 \sim \mathcal{N}(\mathbf{0}, \sigma_0^2 \mathbf{I})$   
3:   for  $i \in \{0, \dots, N-1\}$  do  
4:      $\gamma = \gamma_0$  if  $\sigma_i > \gamma_{\min}$  else 0  
5:      $\hat{\sigma}_i \leftarrow \sigma_i + \gamma \sigma_i$  ▷ Temporarily increase noise level  $\hat{\sigma}_i$   
6:     sample  $\epsilon_i \sim \mathcal{N}(\mathbf{0}, \mathbf{I})$   
7:      $\hat{\mathbf{X}}_i \leftarrow \mathbf{X}_i + \sqrt{\hat{\sigma}_i^2 - \sigma_i^2} \epsilon_i$  ▷ Add new noise to move from  $\sigma_i$  to  $\hat{\sigma}_i$   
8:      $\mathbf{d}_i \leftarrow (\hat{\mathbf{X}}_i - D_\theta^\omega(\hat{\mathbf{X}}_i; \hat{\sigma}_i, \mathbf{A}, \mathbf{z}_S)) / \hat{\sigma}_i$  ▷ Evaluate  $d\mathbf{X}/d\sigma$  at  $\hat{\sigma}_i$   
9:      $\mathbf{X}_{i+1} \leftarrow \hat{\mathbf{X}}_i + (\sigma_{i+1} - \hat{\sigma}_i) \mathbf{d}_i$  ▷ Take Euler step from  $\hat{\sigma}_i$  to  $\sigma_{i+1}$   
10:    if  $\sigma_{i+1} \neq 0$  then  
11:       $\mathbf{d}'_i \leftarrow (\mathbf{X}_{i+1} - D_\theta^\omega(\mathbf{X}_{i+1}; \sigma_{i+1})) / \sigma_{i+1}$  ▷ Apply 2nd order correction  
12:       $\mathbf{X}_{i+1} \leftarrow \hat{\mathbf{X}}_i + (\sigma_{i+1} - \hat{\sigma}_i) (\frac{1}{2} \mathbf{d}_i + \frac{1}{2} \mathbf{d}'_i)$   
13:    end if  
14:  end for  
15:  return  $\mathbf{X}_N$   
16: end procedure
```

Sampling Procedure. The reverse diffusion process begins with $\mathbf{X}_0 \sim \mathcal{N}(\mathbf{0}, \sigma_{\max}^2 \mathbf{I})$ and iteratively denoises to obtain \mathbf{X}_N . This process is governed by the stochastic differential equation (SDE) [32]:

$$d\mathbf{X} = \underbrace{-\sigma \nabla_{\mathbf{X}} \log p(\mathbf{X}; \sigma | \mathbf{A}, \mathbf{z}_S) d\sigma}_{\text{probability flow ODE}} - \underbrace{\beta(\sigma) \sigma^2 \nabla_{\mathbf{X}} \log p(\mathbf{X}; \sigma | \mathbf{A}, \mathbf{z}_S) d\sigma + \sqrt{2\beta(\sigma)} \sigma d\mathbf{w}}_{\text{Langevin diffusion SDE}}, \quad (11)$$

where $\nabla_{\mathbf{X}} \log p(\mathbf{X}; \sigma | \mathbf{A}, \mathbf{z}_S) = (D_\theta^\omega(\mathbf{X}_\sigma; \sigma, \mathbf{A}, \mathbf{z}_S) - \mathbf{X}) / \sigma^2$ is the conditional score function [24], σ is the noise level, and $d\mathbf{w}$ is the Wiener process. The term $\beta(\sigma)$ determines the rate at which existing noise is replaced by new noise.

During inference, the noise level schedule $\sigma_{i \in \{0, \dots, N\}}$ is defined as EDM [32]:

$$\sigma_{i < N} = \left(\sigma_{\max}^{\frac{1}{\rho}} + \frac{i}{N-1} (\sigma_{\min}^{\frac{1}{\rho}} - \sigma_{\max}^{\frac{1}{\rho}}) \right)^\rho, \quad \sigma_N = 0, \quad (12)$$

where $\sigma_{\max} = 80$, $\sigma_{\min} = 0.0004$, $\rho = 7$, and $N = 50$ is the number of diffusion steps. The sampling process is performed by solving the SDE using the stochastic Heun’s 2nd method [32], as outlined in Algorithm 3.

B Details of NMR-DiGress

As introduced in Section 5.2 of the main paper, NMR-DiGress is a graph-based baseline model integrating the discrete graph diffusion model DiGress [66] with our NMR-ConvFormer for molecular structure elucidation from 1D NMR spectra and the chemical formula. In this section, we provide a detailed description of the training and sampling procedures of NMR-DiGress.

In NMR-DiGress, molecule-spectrum pairs are represented as $(\mathcal{G}, \mathcal{S})$, where $\mathcal{G} = (\mathbf{A}, \mathbf{E})$ is the molecular graph. The atom types $\mathbf{A} \in \{0, 1\}^{N \times d_{\text{atom}}}$ and bond types $\mathbf{E} \in \{0, 1\}^{N \times N \times d_{\text{bond}}}$ represent the graph, with N being the number of heavy atoms (excluding hydrogens), and d_{atom} and d_{bond} being the total number of atom and bond types, respectively. Bond types include no bond, single bond, double bond, triple bond, and aromatic bond.

The objective of NMR-DiGress is to generate the bond types \mathbf{E} conditioned on the atom types \mathbf{A} (i.e., chemical formula) and the spectra \mathcal{S} by sampling from the conditional probability distribution $p(\mathbf{E} | \mathbf{A}, \mathcal{S})$. Key differences from the original DiGress are: (1) Atom types are already known in NMR-DiGress, so only bond matrices are predicted. (2) Spectra embeddings \mathbf{z}_S from NMR-ConvFormer are added as graph-level features during training and sampling.

Algorithm 4 NMR-DiGress Training.

```
1: procedure TRAIN NMR-DIGRESS(molecular graph  $\mathcal{G} = (\mathbf{A}, \mathbf{E})$ , NMR spectra embedding  $\mathbf{z}_S$ )
2:   sample  $t \sim \mathcal{U}[1, T]$  ▷ Sample a diffusion time from the uniform distribution
3:   sample  $\mathbf{E}^t \sim \mathbf{E} \bar{\mathbf{Q}}^t$  ▷ Add noise to the bond matrix
4:    $\mathcal{G}^t \leftarrow (\mathbf{A}, \mathbf{E}^t)$ 
5:    $\mathbf{z}_{\mathcal{G}} \leftarrow f(\mathcal{G}^t, t)$  ▷ Structural features computed from the graph
6:    $\hat{\mathbf{p}}^E \leftarrow \phi_{\theta}(\mathcal{G}^t, \mathbf{z}_{\mathcal{G}}, \mathbf{z}_S)$  ▷ Predict the bond matrix
7:   minimize  $\ell_{CE}(\hat{\mathbf{p}}^E, \mathbf{E})$  ▷ Cross-entropy loss
8: end procedure
```

Algorithm 5 NMR-DiGress Sampling.

```
1: procedure SAMPLE NMR-DIGRESS(NMR spectra embedding  $\mathbf{z}_S$ , atom types  $\mathbf{A}$ , marginal distribution of
   bond types  $\mathbf{m}$ , number of diffusion steps  $T$ )
2:   sample  $\mathbf{E}^T \sim \mathbf{m}$  ▷ Independently sample each initial bond from the marginal distribution
3:    $\mathcal{G}^T \leftarrow (\mathbf{A}, \mathbf{E}^T)$ 
4:   for  $t = T, \dots, 1$  do
5:      $\mathbf{z}_{\mathcal{G}} \leftarrow f(\mathcal{G}^t, t)$  ▷ Structural features computed from the graph
6:      $\hat{\mathbf{p}}^E \leftarrow \phi_{\theta}(\mathcal{G}^t, \mathbf{z}_{\mathcal{G}}, \mathbf{z}_S)$  ▷ Predict the bond matrix
7:      $p_{\theta}(e_{ij}^{t-1} | \mathcal{G}^t) \leftarrow \sum_e q(e_{ij}^{t-1} | e_{ij} = e, e_{ij}^t) \hat{p}_{ij}^E(e)$  ▷ Posterior distribution of each bond
8:      $\mathcal{G}^{t-1} \sim \mathbf{A} \times \prod_{ij} p_{\theta}(e_{ij}^{t-1} | \mathcal{G}^t)$  ▷ Reverse process
9:   end for
10:  return  $\mathcal{G}^0$ 
11: end procedure
```

Training Procedure. The training procedure of NMR-DiGress is adapted from DiGress [66]. Noise is added to each bond independently via discrete Markov chains, and a neural network is trained to reverse this process to generate bond matrices.

Specifically, to add noise to a graph, we define a discrete Markov process $\{\mathbf{E}^t\}_{t=0}^T$ starting from the bond matrix $\mathbf{E}^0 = \mathbf{E}$:

$$q(\mathbf{E}^t | \mathbf{E}^{t-1}) = \mathbf{E}^{t-1} \mathbf{Q}^t, \quad (13)$$

where \mathbf{Q}^t is the transition matrix from step $t-1$ to t . From the properties of the Markov chain, the distribution of \mathbf{E}^t given \mathbf{E} is:

$$q(\mathbf{E}^t | \mathbf{E}) = \mathbf{E} \bar{\mathbf{Q}}^t, \quad (14)$$

where $\bar{\mathbf{Q}}^t = \mathbf{Q}^1 \mathbf{Q}^2 \dots \mathbf{Q}^t$. Following DiGress, we use the noise schedule:

$$\bar{\mathbf{Q}}^t = \bar{\alpha}^t \mathbf{I} + \bar{\beta}^t \mathbf{1} \mathbf{m}^{\top}, \quad (15)$$

where $\bar{\alpha}^t = \cos(0.5\pi(t/T + s)/(1+s))^2$, $\bar{\beta}^t = 1 - \bar{\alpha}^t$, $T = 500$ is the number of diffusion steps, and s is a small hyperparameter. Here, \mathbf{m} is the marginal distribution of bond types in the training dataset and \mathbf{m}^{\top} is the transpose of \mathbf{m} . This choice of noise schedule ensures that each bond in \mathbf{E}_T is converged to the prior noisy distribution (i.e., the marginal distribution of bond types \mathbf{m}).

To predict the original bond matrix \mathbf{E} from the noisy graph $\mathcal{G}^t = (\mathbf{A}, \mathbf{E}_t)$, we train a neural network $\phi_{\theta}(\mathcal{G}^t, \mathbf{z}_{\mathcal{G}}, \mathbf{z}_S)$, where $\mathbf{z}_{\mathcal{G}}$ is extra features derived from \mathcal{G}^t in DiGress and \mathbf{z}_S is the NMR spectra embedding from NMR-ConvFormer. We use the same graph transformer architecture as in DiGress for ϕ_{θ} [66]. The complete training algorithm is shown in Algorithm 4.

Sampling Procedure. We extend DiGress [66] by conditioning on atom types \mathbf{A} and spectra embeddings \mathbf{z}_S . Each bond in \mathbf{E}^T is independently sampled from the marginal distribution \mathbf{m} to form the noisy graph $\mathcal{G}^T = (\mathbf{A}, \mathbf{E}^T)$. For each timestep t , we compute extra features $\mathbf{z}_{\mathcal{G}} = f(\mathcal{G}^t, t)$, predict bond probabilities $\hat{\mathbf{p}}^E = \phi_{\theta}(\mathcal{G}^t, \mathbf{z}_{\mathcal{G}}, \mathbf{z}_S)$, and derive the posterior for each bond e_{ij} :

$$p_{\theta}(e_{ij}^{t-1} | \mathcal{G}^t) = \sum_e q(e_{ij}^{t-1} | e_{ij} = e, e_{ij}^t) \hat{p}_{ij}^E(e), \quad (16)$$

where e can be chosen from d_{bond} bond types. Then each bond in \mathcal{G}^{t-1} is independently sampled according to this posterior. After T steps, the denoised molecular graph \mathcal{G}^0 is generated. The complete algorithm is given in Algorithm 5.

C Details of Dataset Curation

In this section, we provide details on the dataset curation process, including the data structure, preprocessing pipeline, and a summary of the statistics for each dataset.

C.1 Dataset Structure and Preprocessing

Each data entry is represented as a tuple (*SMILES*, *¹H NMR spectrum*, *¹³C NMR spectrum*, *atom features*). The SMILES string is a sequence of characters representing a molecule [71]. Each SMILES string is canonicalized, with stereochemistry such as chiral centers and double bond configurations removed. Only molecules containing the elements C, H, O, N, S, P, F, Cl, Br, and I are retained. Duplicate entries are removed to ensure one unique SMILES per molecule.

The NMR spectra are stored as vectors, and details of the preprocessing steps are provided in Appendix C.2. Atom features include atom types *A* and 3 ground-truth conformers *X*, which are generated using RDKit’s ETKDGv3 algorithm [1] from the SMILES string. To validate the generated 3D conformations, SMILES strings are reconstructed from the atom types and 3D coordinates using RDKit’s DetermineBonds function [1]. Molecules that fail reconstruction are discarded. Explicit hydrogens are included to ensure accurate SMILES reconstruction, as required by DetermineBonds.

C.2 NMR Spectrum Preprocessing

Synthetic Spectra Simulation. Synthetic spectra are generated from SMILES using MestreNova [44], with deuterated chloroform (CDCl₃) as the solvent. Default simulation settings are applied: ¹H spectra (−2 ppm to 12 ppm, 32k points, 500.12 Hz frequency, 0.75 Hz line width) and ¹³C spectra (−20 ppm to 230 ppm, 128k points, 125.03 MHz frequency, 1.5 Hz line width, proton decoupled).

Experimental Spectra Collection. SpecTeach [65] experimental raw spectra are in .mnova file format, with default NMR processing steps preserved, including group delay correction, apodization in the time domain, and phase and baseline corrections in the frequency domain if exist. NMRShiftDB2 [34] has ¹³C NMR spectra chemical shift lists.

Spectra Preprocessing. To standardize spectra from different datasets, which vary in chemical shift ranges, resolutions, and intensity scales, we adopt the formats in [4, 22] and the preprocessing method in [22]. ¹H NMR spectra are linearly interpolated to 10,000 points in the range [−2, 10] ppm, and ¹³C NMR spectra are interpolated to 10,000 points in the range [−20, 230] ppm. Spectra outside these ranges are truncated, while shorter spectra are zero-padded. Intensities are normalized by dividing by the maximum intensity. For SpectraBase dataset [22] and experimental datasets, ¹³C NMR spectra are preprocessed into 80 binary vectors spanning (3.42, 231.3) ppm.

To ensure compatibility with baseline models (i.e., Hu et al. [22] and NMR-DiGress), we also preprocess ¹H NMR spectra into 28,000 points within the range [−2, 12] ppm and ¹³C NMR spectra into 80 binary vectors spanning (3.42, 231.3) ppm where applicable. Appendix Table 4 provides detailed preprocessing formats for each model and dataset.

Table 4: Standardized formats for preprocessed NMR spectra, specifying spectrum dimensions, chemical shift ranges, and intensity ranges.

NMR Spectrum	Dimension	Chemical Shift (ppm)	Intensity
CHEFNMR			
¹ H (Default)	10,000	[−2, 10]	≤ 1
¹³ C (USPTO, SpectraNP)	10,000	[−20, 230]	≤ 1
¹³ C (SpectraBase, SpecTeach, NMRShiftDB2)	80	(3.42, 231.3)	{0, 1}
Hu et al. [22]			
¹ H (Default)	28,000	[−2, 12]	≤ 1
¹³ C (Default)	80	(3.42, 231.3)	{0, 1}
¹ H (USPTO)	10,000	[−2, 10]	≤ 1
NMR-DiGress			
¹ H (Default)	10,000	[−2, 10]	≤ 1
¹³ C (Default)	80	(3.42, 231.3)	{0, 1}

Table 5: Summary of dataset statistics with the number of data points, heavy atoms (excluding hydrogens), atoms (including hydrogens), atom types, and solvent types reported.

Dataset	# Data	# Heavy Atoms	# Atoms	Atom Type	Solvent
Synthetic Datasets					
SpectraBase	141,489	[2, 19]	[3, 59]	4 (C, H, O, N)	CDCl ₃
USPTO	744,602	[5, 35]	[8, 101]	10 (C, H, O, N, S, P, F, Cl, Br, I)	CDCl ₃
SpectraNP	111,181	[3, 130]	[4, 274]	10 (C, H, O, N, S, P, F, Cl, Br, I)	CDCl ₃
Experimental Datasets					
SpecTeach	238	[2, 29]	[5, 59]	7 (C, H, O, N, S, Cl, Br)	CDCl ₃ , DMSO
NMRShiftDB2	23,457	[3, 35]	[3, 91]	10 (C, H, O, N, S, P, F, Cl, Br, I)	>7 solvents

C.3 Dataset Statistics

This section provides detailed preprocessing steps and dataset statistics (Appendix Table 5).

Synthetic Datasets. We evaluate our models on two public benchmarks, SpectraBase [22] and USPTO [4], and our self-curated SpectraNP dataset.

SpectraBase [22] contains molecules with elements C, H, O, and N. The original dataset comprises 142,894 tuples of (Canonical nonstereo SMILES, 28,000-dimensional ¹H NMR spectrum, 80-bin ¹³C NMR spectrum) along with non-overlapping split indices in a ratio of 0.8:0.1:0.1 for training, validation, and test sets. Each molecule in the dataset is unique. We remove 219 molecules with invalid ¹H NMR spectra. After generating 3D conformations for all molecules, 141,489 valid conformations remain. The original dataset is available at <https://zenodo.org/records/13892026> under the CC-BY 4.0 license.

USPTO [4] includes molecules derived from chemical reactions [41], containing elements C, H, O, N, S, P, F, Cl, Br, and I. The original dataset contains 794,403 tuples of (Canonical stereo SMILES, 10,000-dimensional ¹H NMR spectrum, 10,000-dimensional ¹³C NMR spectrum). We generate 3D conformations for each molecule. The final dataset contains 744,602 entries. The original split indices are preserved, resulting in a post-filtering split ratio of 0.86:0.04:0.1 for training, validation, and test sets. The original dataset is available at <https://zenodo.org/records/11611178> under the Community Data License Agreement-Sharing 1.0 (CDLA-Sharing-1.0).

SpectraNP contains 111,181 unique natural products with elements C, H, O, N, S, P, F, Cl, Br, and I. Around 31k molecules are sourced from the NPAtlas database [52], which includes small molecules from bacteria and fungi. The remaining molecules are sourced from the NP-MRD database [72], which includes natural products such as vitamins, minerals, probiotics, and small molecules from various natural sources. The dataset is randomly split into training, validation, and test sets in a ratio of 0.8:0.1:0.1.

Experimental Datasets. To evaluate the ability of models trained on synthetic data to generalize to experimental data, we curate two experimental datasets.

SpecTeach includes the van Bramer dataset [65]. The original dataset contains 247 tuples, but 5 compounds lack corresponding SMILES from the CAS ID, and 3 compounds have invalid experimental spectra. The final dataset comprises 238 unique tuples. Most compounds are in CDCl₃ solvent, with a few in DMSO solvent. The original dataset is available at <https://drive.google.com/drive/folders/1R23KGk3bp6ukGCRb4U-CRuxnL6PYYBYc> under CC-BY 4.0.

NMRShiftDB2 [34] is a larger-scale dataset of ¹³C NMR spectra in various solvents. We use a subset of 23,457 molecules excluding SMILES in the training set of USPTO. The original dataset is under the nmrshiftdb2 Database License (<https://nmrshiftdb.nmr.uni-koeln.de/nmrshiftdbhtml/nmrshiftdb2datalicense.txt>).

D Experimental Details

In this section, we provide experimental details for baseline models and CHEFNMR, including hyperparameters, training, and evaluation settings.

D.1 Baseline Settings

We compare CHEFNMR with two existing chemical language models and introduce a graph-based model to evaluate different molecular representations for the structure elucidation task.

Hu et al. [22] use 28,000-dimensional ^1H NMR spectra and 80-bin ^{13}C NMR spectra for all datasets, except for the USPTO dataset, where 10,000-dimensional ^1H NMR spectra are used (see Appendix Table 4). This chemical language model employs a two-stage multitask transformer to predict SMILES strings from raw 1D NMR spectra. The method pre-defines 957 substructures and pre-trains a substructure-to-SMILES transformer model on 3.1M molecules. This pre-trained model is then used to initialize a multitask transformer, which is fine-tuned on 143k data from SpectraBase.

For our experiments, we retrain the substructure-to-SMILES model on the same 3.1M dataset for 500 epochs. Then, we fine-tune the model on each synthetic benchmark dataset for 1500 epochs until convergence. During fine-tuning, the multitask model is initialized with the substructure-to-SMILES transformer checkpoint that achieved the lowest validation loss during the pre-training phase. Model performance is evaluated on each dataset over three independent runs, using the checkpoint with the lowest validation loss during training. Evaluation is conducted on 1 A100 GPU, with runtime varying between 30 minutes and 2 hours depending on the dataset. Other hyperparameters are set as default in the original model [22].

Alberts et al. [4] develop a transformer to predict stereo SMILES from text-based 1D NMR peak lists and chemical formulas. Due to the unavailability of inference code and differences in input (peak lists vs. raw spectra) and output (stereo vs. non-stereo SMILES), we report their published results on the original USPTO (794,403 data points) and SpecTeach datasets.

NMR-DiGress uses 10,000-dimensional ^1H NMR spectra and 80-bin ^{13}C NMR spectra for all datasets (see Appendix Table 4). This graph-based model, comprising 14.4M parameters, is trained on each dataset using 4 A100 GPUs for 48 hours. Evaluation is performed using the checkpoint with the highest top-1 matching accuracy on the validation set.

Notably, molecules containing aromatic nitrogens are excluded from training and evaluation (see Appendix Table 6). This is because NMR-DiGress only uses heavy atoms (excluding hydrogens) as graph nodes, and RDKit [1] fails to reconstruct SMILES strings from molecular graphs with aromatic nitrogens.

Table 6: Number of filtered data.

Dataset	# Data
SpectraBase	132,710
USPTO	673,257
SpectraNP	106,020

D.2 CHEFNMR Settings

CHEFNMR use the preprocessed datasets described in Appendix Tables 4 and 5. Appendix Figure 6 illustrates the full architecture of the NMR-ConvFormer described in Section 3.1. Appendix Table 8 lists the hyperparameters and optimizer settings for CHEFNMR.

All models are trained in bf16-mixed precision. After training, we sample all molecules in the test set using the trained checkpoint for three independent runs per dataset. We select the checkpoint with the highest top-1 matching accuracy on the validation set. For experimental datasets, we use the checkpoint trained on the synthetic USPTO dataset with 10,000-dimensional ^1H NMR spectra and 80-bin ^{13}C NMR spectra. Appendix Table 7 summarizes σ_{data} , training epochs, and sampling time for CHEFNMR on each dataset. Here, σ_{data} represents the standard deviation of the atom coordinates in the dataset. The classifier-free guidance (CFG) scale ω is set to 2 for SpectraBase, 1.5 for USPTO and SpectraNP, and 1 for SpecTeach and NMRShiftDB2.

Table 7: σ_{data} , training epochs, and sampling time per dataset for CHEFNMR. σ_{data} is the standard deviation of the atom coordinates in the dataset. Sampling time is the estimated average time on 1 A100 or H100 GPU for three independent runs.

Dataset	σ_{data}	CHEFNMR-S		CHEFNMR-L	
		Train Epoch	Sample Time	Train Epoch	Sample Time
SpectraBase	2.02	10k	1h	5k	3h
USPTO	2.67	10k	8h	3k	17h
SpectraNP	3.28	26k	3.5h	18k	9h

Table 9: Ablation study on NMR-ConvFormer components.

Configuration	Tokenizer	# Tokens	Transformer	Pooling	Dropout	Acc@1% \uparrow	Sim@1 \uparrow
Base (CHEFNMR-S)	Conv	183	Y	MAP	0.1	69.15\pm.08	0.807\pm.002
Tokenizer Ablation							
– Conv Tokenizer	Patch	183	Y	MAP	0.1	61.78 \pm .18	0.756 \pm .000
– Token Count Reduction	Conv	121	Y	MAP	0.1	66.28 \pm .18	0.789 \pm .001
Transformer Ablation							
– Transformer Block	Conv	183	N	MAP	0.1	68.12 \pm .17	0.797 \pm .001
Pooling Ablation							
– MAP Pooling	Conv	183	Y	Flatten	0.1	62.97 \pm .14	0.758 \pm .002
Dropout Ablation							
– Dropout	Conv	183	Y	MAP	0.0	65.48 \pm .06	0.777 \pm .001

E Additional Ablation Studies

In this section, we provide additional ablation studies to evaluate the impact of the NMR-ConvFormer components and the impact of different NMR spectra on CHEFNMR’s performance.

E.1 Ablation Studies for NMR-ConvFormer

We perform extensive ablation studies to evaluate the contributions of key components in the NMR-ConvFormer on the SpectraBase dataset using CHEFNMR-S. The results are summarized in Table 3 of the main paper, with detailed configurations provided here.

Some of the modifications in Appendix Table 9 are: – **Conv Tokenizer**: The convolutional tokenizer is replaced with a patch tokenizer (see Appendix Figure 6) using `patch_size = 192` and `stride = 96` to maintain the same token count. – **Token Count Reduction**: The number of tokens is reduced from 183 to 121 by increasing max pooling sizes (`pool_size` in Appendix Table 8) from [8, 12] to [12, 20]. – **MAP Pooling**: The MAP pooling layer is replaced with a flattening layer, which reshapes the transformer encoder’s output from $(\text{batch_size}, T, D_{\text{encoder}})$ to $(\text{batch_size}, T \times D_{\text{encoder}})$.

We find that within the NMR-ConvFormer, the convolutional tokenizer outperforms the patch tokenizer, likely due to its ability to capture local features more effectively. Reducing the number of tokens leads to a drop in performance. The MAP pooling layer is more effective than flattening for aggregating features. Dropout regularization is necessary to prevent overfitting.

E.2 Ablation Studies for Different NMR Spectra

We investigate the impact of using different NMR spectra (^1H NMR, ^{13}C NMR, or both) on model performance on the SpectraBase dataset. The results are presented in Appendix Table 10. CHEFNMR

Table 10: Performance on SpectraBase using different NMR spectra.

Spectrum	Model	Top-1		Top-5		Top-10	
		Acc% \uparrow	Sim \uparrow	Acc% \uparrow	Sim \uparrow	Acc% \uparrow	Sim \uparrow
^{13}C	Hu et al.	4.50 \pm .15	0.296 \pm .000	12.92 \pm .11	0.460 \pm .001	18.27 \pm .14	0.523 \pm .001
	NMR-DiGress	10.87 \pm .08	0.314 \pm .001	19.35 \pm .03	0.438 \pm .001	23.00 \pm .02	0.477 \pm .001
	CHEFNMR-S	26.69 \pm .06	0.469 \pm .001	39.90 \pm .33	0.612 \pm .001	44.59 \pm .07	0.651 \pm .000
	CHEFNMR-L	30.28\pm.15	0.510\pm.002	47.33\pm.14	0.672\pm.000	53.53\pm.30	0.718\pm.001
^1H	Hu et al.	31.12 \pm .15	0.569 \pm .001	48.64 \pm .42	0.725 \pm .001	54.92 \pm .26	0.771 \pm .001
	NMR-DiGress	31.13 \pm .13	0.521 \pm .001	48.73 \pm .24	0.682 \pm .001	54.52 \pm .18	0.723 \pm .001
	CHEFNMR-S	57.97 \pm .25	0.720 \pm .002	72.64 \pm .22	0.841 \pm .002	76.58 \pm .23	0.867 \pm .002
	CHEFNMR-L	59.37\pm.20	0.739\pm.001	74.91\pm.11	0.857\pm.001	79.20\pm.09	0.884\pm.000
$^{13}\text{C} + ^1\text{H}$	Hu et al.	45.24 \pm .18	0.686 \pm .001	62.37 \pm .08	0.815 \pm .001	67.38 \pm .05	0.847 \pm .001
	NMR-DiGress	43.56 \pm .30	0.625 \pm .002	62.47 \pm .20	0.779 \pm .002	68.39 \pm .35	0.817 \pm .001
	CHEFNMR-S	69.15 \pm .08	0.807 \pm .002	82.09 \pm .24	0.904 \pm .002	85.30 \pm .04	0.922 \pm .000
	CHEFNMR-L	72.04\pm.02	0.833\pm.000	85.24\pm.10	0.923\pm.001	88.20\pm.07	0.940\pm.000

consistently and significantly outperforms the baselines with ^1H or/and ^{13}C spectra. The combination of ^1H and ^{13}C spectra provides complementary information that yields the best performance.

F Additional Results and Analysis

This section provides additional results and analysis across datasets, demonstrating the state-of-the-art performance and generalization ability of CHEFNMR. Appendix F.1 reports the Average Minimum RMSD metrics for generated 3D structures. Appendix F.2 analyzes CHEFNMR’s generalization ability to unseen molecular scaffolds and different solvents in NMR spectra. Appendix F.3 presents a systematic failure mode analysis of CHEFNMR by molecular structures and domain shift between synthetic and real spectra. Appendix F.4 and F.5 provide additional qualitative examples on synthetic and experimental datasets respectively.

F.1 RMSD Metric

Since CHEFNMR generates atomic 3D coordinates, we additionally report the top- k Average Minimum RMSD (AMR) of heavy atoms in Appendix Table 11. The RMSD for each predicted structure is computed against three ground-truth conformers and taken as the minimum value. We then select the minimum RMSD among the top- k predictions for each molecule and average across all molecules to obtain the top- k AMR. Although RMSD is not size-independent and thus less interpretable, the obtained results are reasonable given the dataset complexity.

Table 11: Average Minimum RMSD in Å.

Dataset	Top-1↓	Top-5↓	Top-10↓
SpectraBase	3.26	2.87	2.71
USPTO	4.59	4.14	3.96
SpectraNP	5.50	5.12	4.97
SpecTeach	2.10	1.71	1.56
NMRShiftDB2	3.23	2.83	2.68

F.2 Generalization Analysis

In this section, we analyze CHEFNMR’s generalization ability to unseen molecular scaffolds (Appendix F.2.1) and different solvents (Appendix F.2.2) in NMR spectra.

F.2.1 Generalization to Unseen Molecular Scaffolds

We evaluate CHEFNMR’s generalization ability to unseen molecular scaffolds by creating test subsets with scaffolds not present in the training sets. Appendix Table 12 shows the subsets are relatively chemically dissimilar to the training sets, based on Scaffold similarity (Scaff), fingerprint-based Tanimoto Similarity to a nearest neighbor (SNN) [51], and the absolute difference of standard deviation of

Table 12: Similarity analysis between training and test splits across datasets. Unseen: test subsets with scaffolds unseen during training. Scaff: Scaffold similarity; SNN: Tanimoto similarity to nearest neighbor. $|\sigma_{\text{train}} - \sigma_{\text{test}}|$: absolute difference of std of atom coordinates between training and test sets.

Train Set	Test (Sub)set	#Test Set Data	Scaff↑	SNN↑	$ \sigma_{\text{train}} - \sigma_{\text{test}} $ ↓
SpectraBase	SpectraBase	14137	0.959	0.659	0.004
SpectraBase	SpectraBase (Unseen)	3770 (26.7%)	0.000	0.657	0.025
USPTO	USPTO	73059	0.980	0.698	0.005
USPTO	USPTO (Unseen)	14711 (20.1%)	0.000	0.656	0.174
SpectraNP	SpectraNP	10952	0.894	0.722	0.012
SpectraNP	SpectraNP (Unseen)	2897 (26.5%)	0.000	0.655	0.144

Table 13: Performance on unseen scaffold test subsets across synthetic datasets.

Dataset	Model	Top-1		Top-5		Top-10	
		Acc% \uparrow	Sim \uparrow	Acc% \uparrow	Sim \uparrow	Acc% \uparrow	Sim \uparrow
SpectraBase	Hu et al.	39.59 \pm .26	0.653 \pm .002	55.43 \pm .64	0.776 \pm .003	59.85 \pm .59	0.807 \pm .003
	NMR-DiGress	43.10 \pm .29	0.607 \pm .003	59.70 \pm .22	0.759 \pm .001	64.83 \pm .24	0.793 \pm .002
	CHEFNMR-S	64.09 \pm .32	0.758 \pm .003	77.35 \pm .20	0.871 \pm .001	80.73 \pm .22	0.892 \pm .001
	CHEFNMR-L	66.40\pm.31	0.785\pm.002	80.24\pm.33	0.891\pm.001	83.75\pm.24	0.912\pm.001
USPTO	Hu et al.	25.80 \pm .22	0.590 \pm .001	41.58 \pm .27	0.738 \pm .001	47.12 \pm .27	0.778 \pm .002
	NMR-DiGress	12.93 \pm .23	0.388 \pm .003	25.27 \pm .22	0.596 \pm .002	31.42 \pm .12	0.653 \pm .001
	CHEFNMR-S	66.68 \pm .04	0.814 \pm .002	81.31 \pm .08	0.921 \pm .000	84.81 \pm .04	0.938\pm.000
	CHEFNMR-L	67.78\pm.25	0.836\pm.003	81.79\pm.11	0.925\pm.000	85.26\pm.13	0.941\pm.001
SpectraNP	Hu et al.	7.68 \pm .36	0.478\pm.001	16.16 \pm .27	0.623 \pm .001	20.26 \pm .27	0.659 \pm .000
	NMR-DiGress	1.59 \pm .10	0.222 \pm .004	4.50 \pm .24	0.389 \pm .002	6.18 \pm .19	0.436 \pm .001
	CHEFNMR-S	21.40 \pm .44	0.417 \pm .001	35.30 \pm .20	0.641 \pm .001	40.14 \pm .09	0.696 \pm .000
	CHEFNMR-L	21.82\pm.24	0.477\pm.002	37.04\pm.66	0.694\pm.001	42.69\pm.31	0.741\pm.002

atom coordinates between training and test sets. Appendix Table 13 shows the performance on these unseen scaffold subsets with different models. CHEFNMR still significantly outperforms baselines across these subsets, demonstrating its generalization ability.

F.2.2 Generalization Across Solvents in Experimental Spectra

We report top-10 zero-shot accuracy on 2k experimental ^{13}C spectra paired with solvent information from NMRShiftDB2 [34] in Appendix Table 14. CHEFNMR trained on synthetic ^{13}C spectra with CDCl_3 solvent shows generalization ability to various solvents except for $\text{C}_5\text{D}_5\text{N}$ and CD_3CN .

Table 14: Top-10 zero-shot accuracy of CHEFNMR on NMRShiftDB2 [34] across different solvents.

Solvent	#Molecules	Top-10 Zero-shot Accuracy
CDCl_3	1498	0.263
DMSO	232	0.323
CD_3OD	197	0.102
$\text{C}_5\text{D}_5\text{N}$	57	0.035
C_6D_6	48	0.188
D_2O	36	0.500
CCl_4	33	0.788
CD_3CN	11	0.000
$(\text{CD}_3)_2\text{CO}$	2	0.500

F.3 Failure Mode Analysis

In this section, we systematically analyze the failure modes of CHEFNMR by molecular structures (Appendix F.3.1) and domain shift between synthetic and real spectra (Appendix F.3.2).

F.3.1 Failure Mode by Molecular Structures

Failure rate is defined as the proportion of molecules where the model fails to generate the correct structure within the top-10 predictions. We analyze the failure rate by molecular structures, including the number of atoms, number of rings, largest ring size, and functional groups of our CHEFNMR on the synthetic SpectraNP (Appendix Table 15 and 16), and experimental SpecTeach (Appendix Table 17 and 18) and NMRShiftDB2 (Appendix Table 19 and 20) datasets.

On all datasets, the model fails more often on molecules with the most atoms or the largest number of rings due to less training data and increasing complexity of spectra and structures for larger molecules. However, the model is not systematically significantly failing in a specific functional group category.

Table 15: Failure rate analysis on synthetic SpectraNP dataset by molecular properties.

By Total Atoms (including hydrogens)						
Total Atoms	≤40	41–80	81–120	121–160	161–200	>200
Total Molecules	2265	6168	1818	539	140	22
Failure Rate	0.296	0.315	0.411	0.492	0.707	1.000
By Heavy Atoms						
Heavy Atoms	≤20	21–40	41–60	61–80	81–100	>100
Total Molecules	2099	6563	1750	415	110	15
Failure Rate	0.298	0.311	0.431	0.542	0.773	1.000
By Number of Rings						
Ring Count	0	1–2	3–4	5–6	7–8	>8
Total Molecules	559	3070	4437	2102	560	224
Failure Rate	0.250	0.317	0.332	0.381	0.407	0.571
By Largest Ring Size						
Largest Ring	No rings	3–5	6	7–8	>8	
Total Molecules	559	483	8061	778	1071	
Failure Rate	0.250	0.383	0.322	0.382	0.490	

Table 16: Failure rate by functional groups on synthetic SpectraNP dataset.

Category	Carbonyls	Amides	Esters	Ethers	Alcohols	Halogen	Sulfur	Nitrogen
Total Molecules	8148	1479	4389	8048	6861	477	138	3046
Failure Rate	0.352	0.411	0.354	0.342	0.355	0.356	0.341	0.386

Table 17: Failure rate analysis on experimental SpecTeach dataset by molecular properties.

By Total Atoms (including hydrogens)						
Total Atoms	≤10	11–15	16–20	21–25	26–30	>30
Total Molecules	10	60	76	48	26	18
Failure Rate	0.000	0.217	0.289	0.271	0.500	0.556
By Heavy Atoms						
Heavy Atoms	≤5	6–10	11–15	16–20	>25	
Total Molecules	38	154	37	8	1	
Failure Rate	0.105	0.240	0.676	0.500	1.000	
By Number of Rings						
Ring Count	0		1		>1	
Total Molecules	157		69		12	
Failure Rate	0.210		0.449		0.583	
By Largest Ring Size						
Largest Ring	No rings		3–5		6	
Total Molecules	157		4		77	
Failure Rate	0.210		0.250		0.481	

Table 18: Failure rate by functional groups on experimental SpecTeach dataset.

Category	Carbonyls	Amides	Esters	Ethers	Alcohols	Halogen	Nitrogen
Total Molecules	125	3	46	58	43	24	24
Failure Rate	0.304	0.667	0.435	0.448	0.256	0.208	0.542

Table 19: Failure rate analysis on experimental NMRShiftDB2 dataset by molecular properties.

By Total Atoms (including hydrogens)					
Total Atoms	≤20	21–40	41–60	61–80	>80
Total Molecules	6484	13685	2806	417	65
Failure Rate	0.351	0.689	0.916	0.947	0.985
By Heavy Atoms					
Heavy Atoms	≤10	11–20	21–30	>30	
Total Molecules	5591	13855	3504	507	
Failure Rate	0.326	0.664	0.917	0.982	
By Number of Rings					
Ring Count	0	1–2	3–4	5–6	7–8
Total Molecules	2955	14763	5192	514	33
Failure Rate	0.334	0.592	0.862	0.977	1.000
By Largest Ring Size					
Largest Ring	No rings	3–5	6	7–8	>8
Total Molecules	2955	3031	16552	682	237
Failure Rate	0.334	0.630	0.666	0.871	0.916

Table 20: Failure rate by functional groups on experimental NMRShiftDB2 dataset.

Category	Carbonyls	Amides	Esters	Ethers	Alcohols	Halogen	Sulfur	Nitrogen
Total Molecules	11096	2562	4320	9699	3756	6248	1207	12074
Failure Rate	0.681	0.713	0.726	0.723	0.759	0.528	0.725	0.674

F.3.2 Domain Shift between Synthetic and Real Spectra

To quantify the domain shift between synthetic and real spectra, we simulate synthetic spectra for molecules in the SpecTeach dataset using MestReNova, and compute the cosine similarity between synthetic and real spectra following [4]. We also report the average cosine similarity of successful and failed predictions on the SpecTeach. Appendix Table 21 shows that 10,000-dimensional ^1H NMR spectra have significantly lower cosine similarity than 80-bin ^{13}C NMR spectra, indicating a need for more robust representation of ^1H NMR spectra. In addition, failed predictions have lower similarity between synthetic and real ^1H spectra. We note that it is non-trivial to develop systematic metrics to quantify the spectra domain shift, and we leave it to future work.

Table 21: Cosine similarity between synthetic and experimental spectra of molecules in SpecTeach, and successful and failed predictions by CHEFNMR.

Type	Count	Cos Sim (^1H)	Cos Sim (^{13}C)
All	238	$0.174 \pm .195$	$0.743 \pm .214$
Success	167	$0.197 \pm .199$	$0.747 \pm .206$
Fail	71	$0.119 \pm .177$	$0.735 \pm .234$

F.4 Additional Qualitative Results on Synthetic Spectra

We present more examples of CHEFNMR’s predictions on the synthetic SpectraBase dataset (Appendix Figure 7), the synthetic USPTO dataset (Appendix Figure 8), and the synthetic SpectraNP dataset (Appendix Figure 9). The quantitative results demonstrate that CHEFNMR effectively elucidates diverse chemical structures across various synthetic datasets.

F.5 Additional Qualitative Results on Experimental Spectra

We present additional examples of CHEFNMR’s zero-shot predictions on experimental datasets, including the SpecTeach dataset (Appendix Figure 10) and the NMRShiftDB2 dataset (Appendix Figure 11). These results highlight CHEFNMR’s robustness to experimental variability, such as differences in solvents, impurities, and baseline noise.

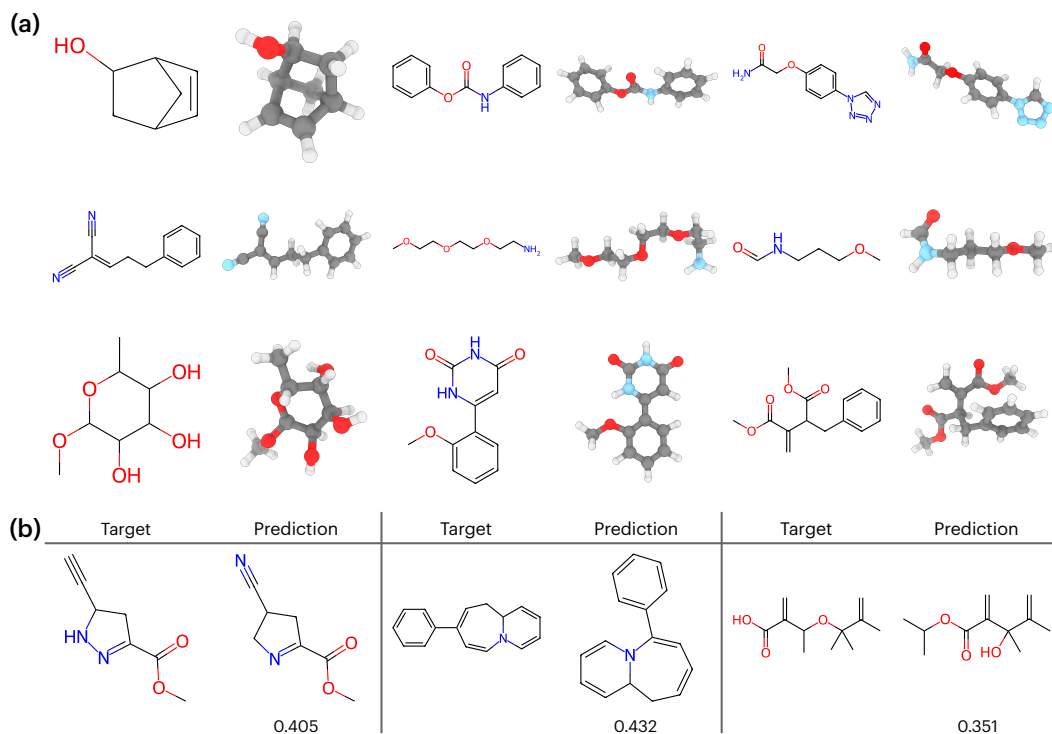


Figure 7: Examples of CHEFNMR’s predictions on the synthetic SpectraBase dataset. **(a)** Correctly predicted structures in top-1 predictions. **(b)** Incorrect top-1 predictions with corresponding Tanimoto similarity scores.

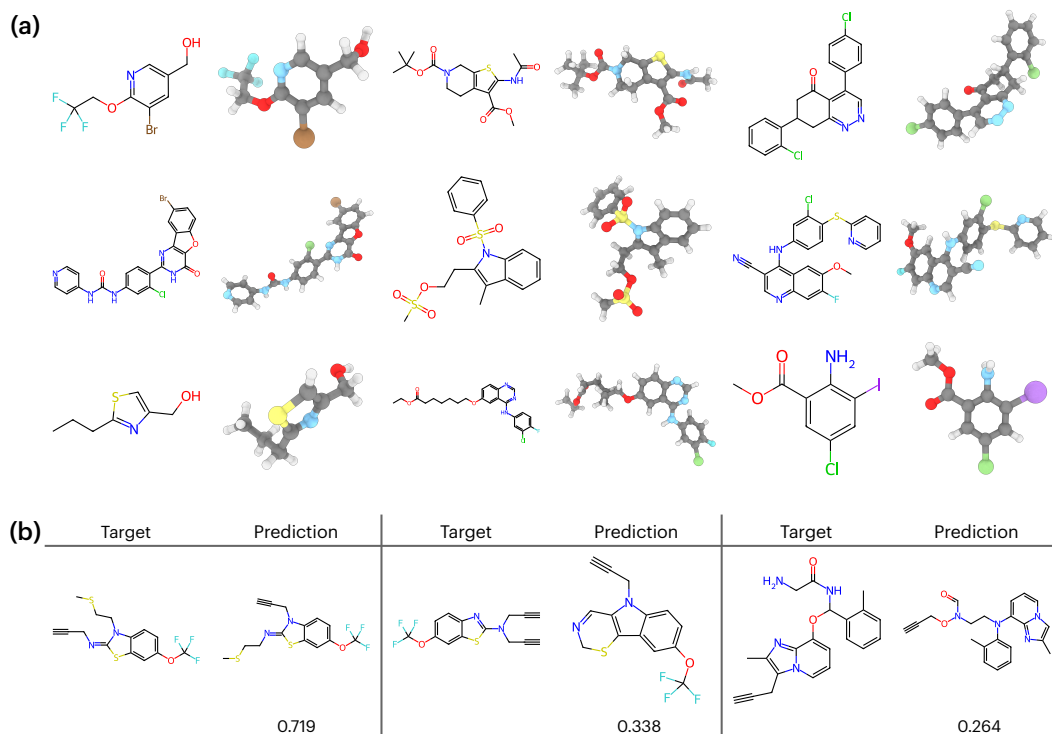


Figure 8: Examples of CHEFNMR’s predictions on the synthetic USPTO dataset. **(a)** Correctly predicted structures in top-1 predictions. **(b)** Incorrect top-1 predictions with corresponding Tanimoto similarity scores.

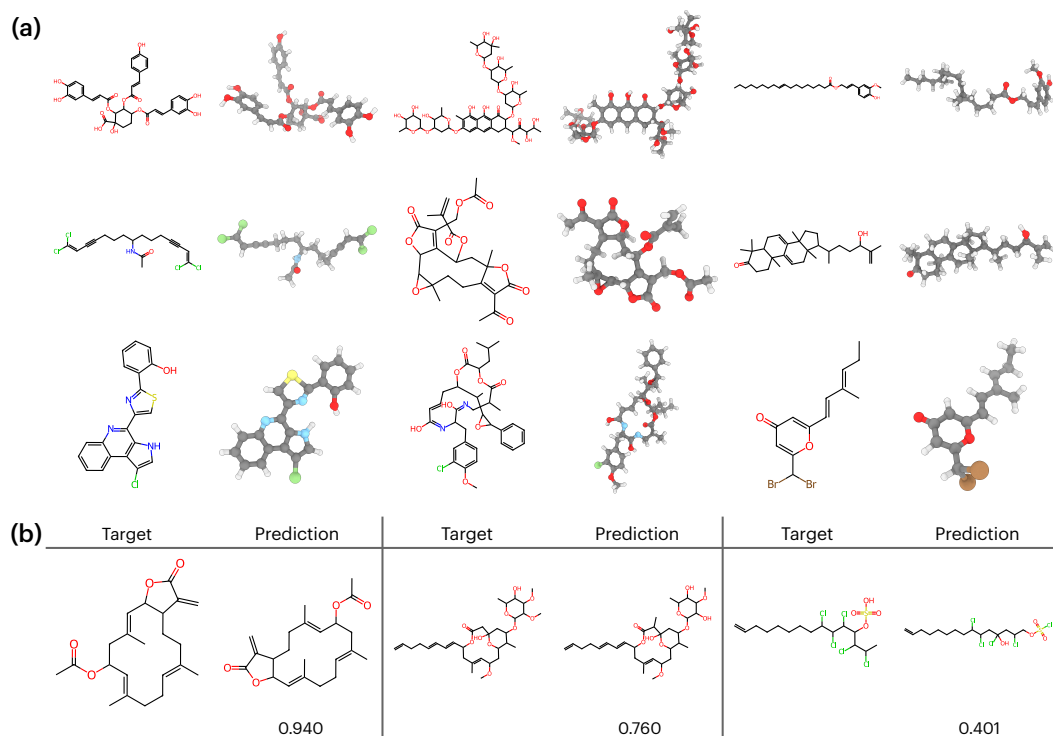


Figure 9: Additional examples of CHEFNMR's predictions on the synthetic SpectraNP dataset. **(a)** Correctly predicted structures in top-1 predictions. **(b)** Incorrect top-1 predictions with corresponding Tanimoto similarity scores.

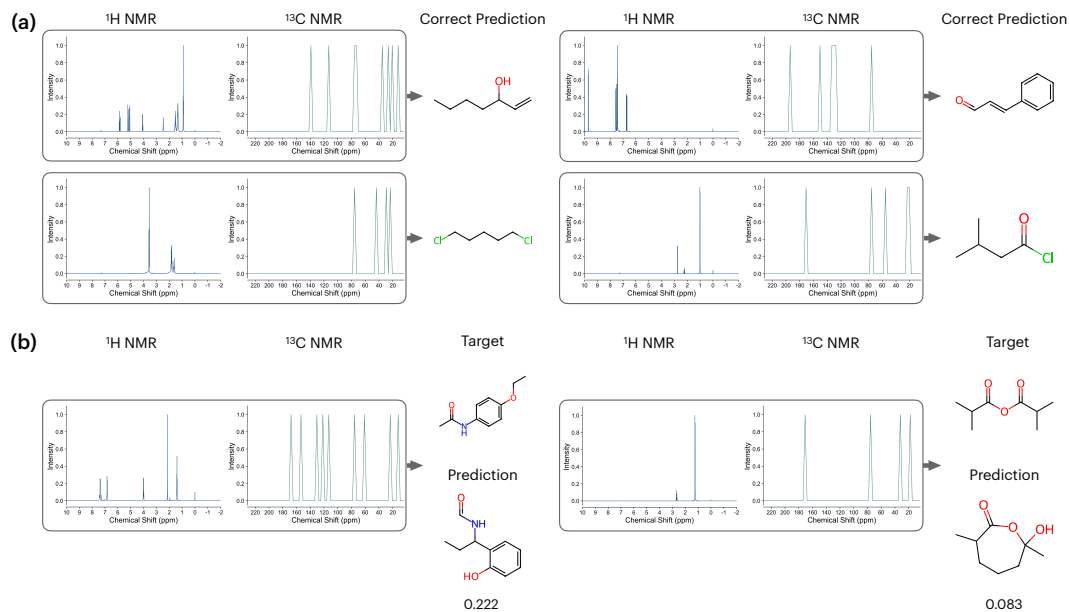


Figure 10: Examples of experimental spectra from the SpecTeach dataset and corresponding CHEFNMR predictions. **(a)** Correct top-1 predictions. **(b)** Incorrect top-1 predictions with corresponding Tanimoto similarity scores.

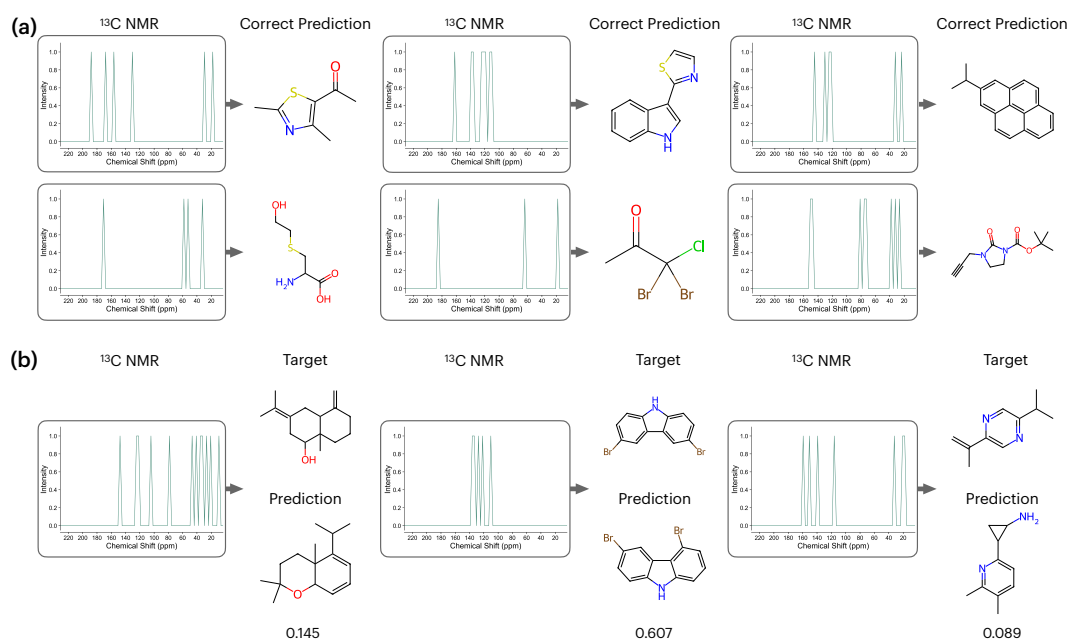


Figure 11: Examples of experimental spectra from the NMRShiftDB2 dataset and corresponding CHEFNMR predictions. **(a)** Correct top-1 predictions. **(b)** Incorrect top-1 predictions with corresponding Tanimoto similarity scores.